Tectonophysics 644–645 (2015) 197–219

Contents lists available at ScienceDirect

Tectonophysics

journal homepage: www.elsevier.com/locate/tecto

A paleolatitude reconstruction of the South Armenian Block (Lesser Caucasus) for the Late Cretaceous: Constraints on the Tethyan realm

Maud J.M. Meijers [a,b,*], Brigitte Smith [c], Uwe Kirscher [d], Marily Mensink [e], Marc Sosson [a], Yann Rolland [a], Araik Grigoryan [f], Lilit Sahakyan [f], Ara Avagyan [f], Cor Langereis [e], Carla Müller [g]

[a] Université de Nice Sophia Antipolis, UMR Géoazur, CNRS, IRD, Observatoire de la Côte d'Azur, 250 rue Albert Einstein, 06560 Valbonne, France
[b] University of Minnesota, Dept of Earth Sciences, 291 Shepherd Labs, 100 Union Street SE, Minneapolis, MN 55455, USA
[c] Université Montpellier 2, INSU-CNRS, Laboratoire Géosciences Montpellier, place E. Bataillon, 34095 Montpellier cedex 5, France
[d] Ludwig-Maximilians-Universität München, Department of Earth and Environmental Sciences, Theresienstrasse 41, 80333 München, Germany
[e] Utrecht University, Paleomagnetic Laboratory 'Fort Hoofddijk', Faculty of Geosciences, Budapestlaan 17, 3584CD Utrecht, The Netherlands
[f] Institute of Geological Sciences, National Academy of Sciences of Armenia, 24a Baghramian avenue, Yerevan 0019, Armenia
[g] PL 66-431 Santok, Ludzislawice, Poland

ARTICLE INFO

Article history:
Received 21 July 2014
Received in revised form 10 January 2015
Accepted 31 January 2015
Available online 7 February 2015

Keywords:
Paleomagnetism
Tethys reconstructions
South Armenian Block
Lesser Caucasus
Inclination shallowing
Collision zone

ABSTRACT

The continental South Armenian Block – part of the Anatolide–Tauride South Armenian microplate – of Gondwana origin rifted from the African margin after the Triassic and collided with the Eurasian margin after the Late Cretaceous. During the Late Cretaceous, two northward dipping subduction zones were simultaneously active in the northern Neo-Tethys between the South Armenian Block in the south and the Eurasian margin in the north: oceanic subduction took place below the continental Eurasian margin and intra-oceanic subduction resulted in ophiolite obduction onto the South Armenian Block in the Late Cretaceous.
The paleolatitude position of the South Armenian Block before its collision with Eurasia within paleogeographic reconstructions is poorly determined and limited to one study. This earlier study places the South Armenian Block at the African margin in the Early Jurassic. To reconstruct the paleolatitude history of the South Armenian Block, we sampled Upper Devonian–Permian and Cretaceous sedimentary rocks in Armenia. The sampled Paleozoic rocks have likely been remagnetized. Results from two out of three sites sampled in Upper Cretaceous strata pass fold tests and probably all three carry a primary paleomagnetic signal. The sampled sedimentary rocks were potentially affected by inclination shallowing. Therefore, two sites that consist of a large number of samples (>100) were corrected for inclination shallowing using the elongation/inclination method.
These are the first paleomagnetic data that quantify the South Armenian Block's position in the Tethys ocean between post-Triassic rifting from the African margin and post-Cretaceous collision with Eurasia. A locality sampled in Lower Campanian Eurasian margin sedimentary rocks and corrected for inclination shallowing, confirms that the corresponding paleolatitude falls on the Eurasian paleolatitude curve. The north–south distance between the South Armenian Block and the Eurasian margin just after Coniacian–Santonian ophiolite obduction was at most 1000 km.

1. Introduction

The Tethys ocean was wedged between the northern and southern domains of the youngest supercontinent Pangea. Breakup of the supercontinent started in the earliest Jurassic (~200 Ma) by opening of the central Atlantic ocean (Deenen et al., 2010; Dietz, 1961; Heezen, 1960; Labails et al., 2010; Müller et al., 1993; Norton, 2000; Richards et al., 1989; Sahabi et al., 2004). Simultaneously, continental fragments such as the Anatolide–Tauride South Armenian (ATA) microplate rifted off the African margin and converged with Eurasia, relics of which presently occupy large parts of the region from Turkey to Armenia. Plate circuits based on paleomagnetic data show that Africa and Eurasia started converging after ~200 Ma (Besse and Courtillot, 2002; Torsvik et al., 2012) and rifting along the African margin was accommodated by subduction below the southern Eurasian margin and within the Tethys ocean. Rifting of the ATA microplate from the African margin resulted in opening the southern branch of Neo-Tethys to its south (Barrier and Vrielynck, 2008). It collided with the Eurasian margin in the Paleocene to Eocene, closing the northern branch of the Neo-Tethys ocean to its north (Robertson et al., 2014; Sosson et al., 2010). The northeastern part of ATA is presently located in the Lesser Caucasus at the former southern Eurasian continental margin (Fig. 1). This northeastern part

* Corresponding author at: University of Minnesota, Dept of Earth Sciences, 291 Shepherd Labs, 100 Union Street SE, Minneapolis, MN 55455, USA. Tel.: +1 612 607 3546.
E-mail address: meijersmaud@gmail.com (M.J.M. Meijers).

http://dx.doi.org/10.1016/j.tecto.2015.01.012
0040-1951/

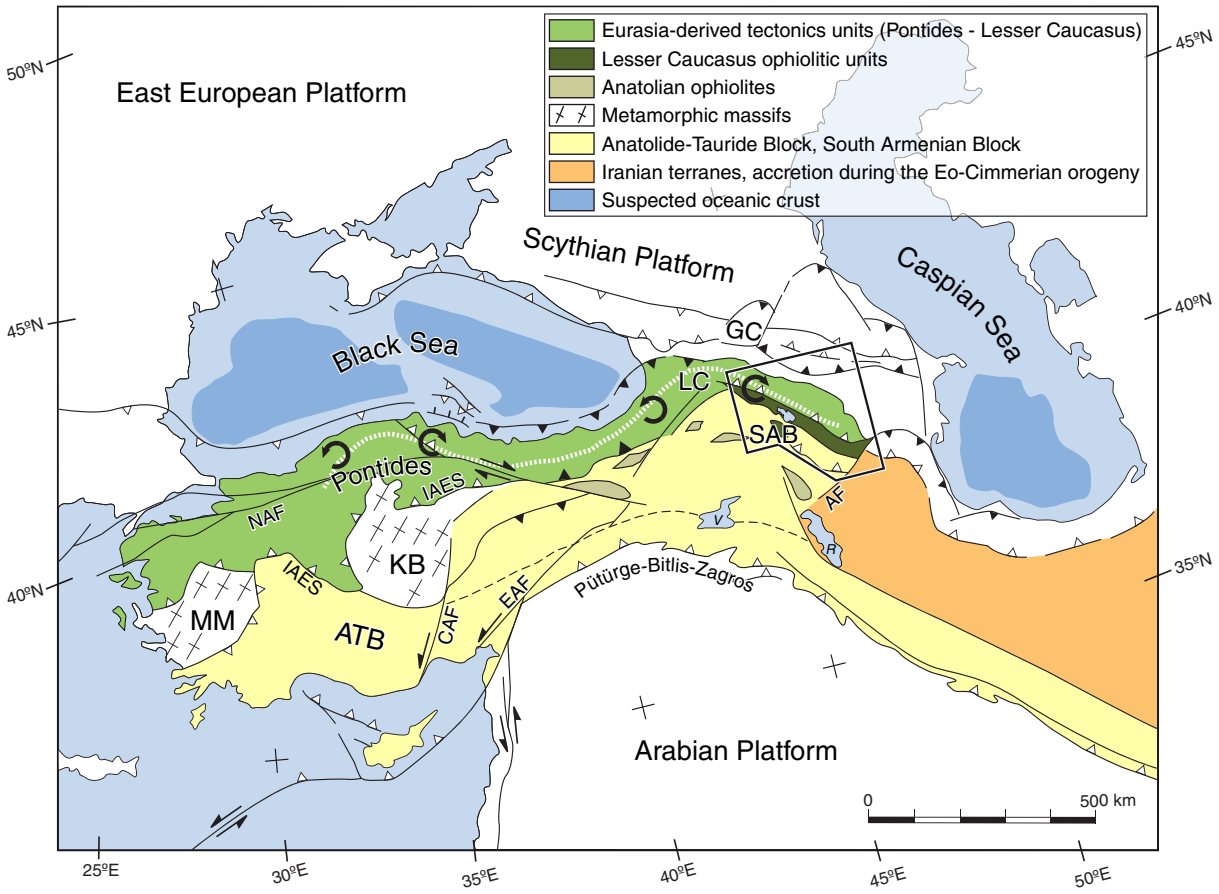

Fig. 1. Tectonic map of the Black and Caspian sea region. AF = Arax Fault, ATB = Anatolide–Tauride Block, CAF = Central Anatolian Fault, EAF = East Anatolian Fault, IAES = Izmir–Ankara–Erzincan suture, KB = Kırşehir Block, GC = Greater Caucasus, LC = Lesser Caucasus, MM = Menderes Massif, NAF = North Anatolian Fault, R = Lake Rezaiyeh, SAB = South Armenian Block, V = Lake Van. Dotted white line roughly indicates the trace of the oroclines through the central Pontides and eastern Pontides–Lesser Caucasus. Black circular arrows in the central Pontides and eastern Pontide–Lesser Caucasus indicate the sense of rotation in both limbs of the orocline. The central Pontide orocline formed in the latest Cretaceous to Early Paleocene (Meijers et al., 2010c). Formation of the eastern Pontides–Lesser Caucasus orocline postdates Eocene time (Bazhenov and Burtman, 2002).

of ATA is generally referred to as the South Armenian Block (SAB; Knipper and Khain, 1980; Monin and Zonenshain, 1987). We mostly refer to the SAB in this paper, because we present data from the Armenian Lesser Caucasus.

There is no clear geologic evidence for the timing of rifting of the SAB from the African margin. Recently Hässig et al. (2014) presented structural, metamorphic and isotopic age data that imply southward subduction below the SAB from ~160 to 123 Ma (Late Jurassic to Early Cretaceous). The forces related to this subduction zone could have driven SAB–Africa rifting. A paleomagnetic study carried out on Jurassic volcanic rocks of the SAB (Bazhenov et al., 1996) gives quantitative constraints and shows that the SAB was positioned at the African margin in the Early Jurassic. Typical errors in paleomagnetic data sets (at best several degrees in paleolatitude or ~300–500 km) would not allow the recognition of an early rifting stage in the Early Jurassic. Therefore rifting is generally assumed to have started during or after the Early Jurassic. No paleomagnetic data constrain the position of the SAB in the Tethys ocean after rifting from the African margin initiated. Closure of the northern branch of the Neo-Tethyan ocean located between the SAB and the Eurasian margin was a two-stage process (Rolland et al., 2009a; Sosson et al., 2010). Northward directed intra-oceanic subduction north of the SAB led to calc-alkaline back-arc magmatism followed by ophiolite obduction onto the SAB (Galoyan et al., 2007; Hässig et al., 2013) in the Cenomanian to Santonian time interval (Danelian et al., 2014; Sosson et al., 2010). From the Middle Jurassic to the Late Cretaceous one other northward dipping subduction zone was active south of Eurasia, resulting in large volume magmatic activity on the active Eurasian margin (the Somkheto–Karabakh island arc; Fig. 1; Adamia et al., 1980). Consumption of the northern Neo-Tethyan oceanic lithosphere finally led to the collision of the SAB with Eurasia.

Sosson et al. (2010) propose a Paleocene age for the start of collision, based on tectonostratigraphic evidence. Middle Eocene strata unconformably cover the SAB, the ophiolitic Sevan–Akera (or Sevan–Hakari) suture zone and the Eurasian margin, marking the amalgamation of the SAB with Eurasia. Okay and Şahintürk (1997), Robinson et al. (1995) and Robertson et al. (2014) propose a Paleocene to Eocene collision age based on the tectonostratigraphy of the eastern Pontides. A significantly older (Campanian) collision age is proposed by Rolland et al. (2009a, 2012), founded on the presence of Eurasian basement-derived blocks in the Coniacian–Santonian formations on top of the obducted ophiolite and on the onset of subduction to the south of the ATA microplate around 95 Ma. Evidence for active subduction from continuing arc magmatism on the Eurasian margin during the Maastrichtian in the Lesser Caucasus (Adamia et al., 2011) and the Paleocene in the eastern Pontides (Altherr et al., 2008; Okay and Şahintürk, 1997), however, contradicts an older Campanian collision.

To reconstruct Tethyan plate kinematics through time, paleomagnetic data from continental blocks (such as the SAB) that do not move independently within the Tethyan ocean could provide a paleo-age grid of the Tethys ocean. Reconstructions of the western Tethyan realm are a challenge due to the limited north–south width of the Tethys ocean that leads to resolution issues when comparing paleomagnetic data from continental blocks and latitude–age curves and their associated errors of the major continents. Here, we present paleomagnetic data from the SAB and its sedimentary cover from Upper Devonian to Upper Cretaceous rocks as well as paleomagnetic data from Upper Cretaceous sedimentary

rocks from the Eurasian margin. The Devonian to Triassic sedimentary rocks were probably remagnetized. Results from the Upper Cretaceous sedimentary rocks were corrected for inclination shallowing and compared to the position of the Eurasian and African margins in order to quantify the position of the SAB within the Tethyan realm and to estimate the age of collision initiation.

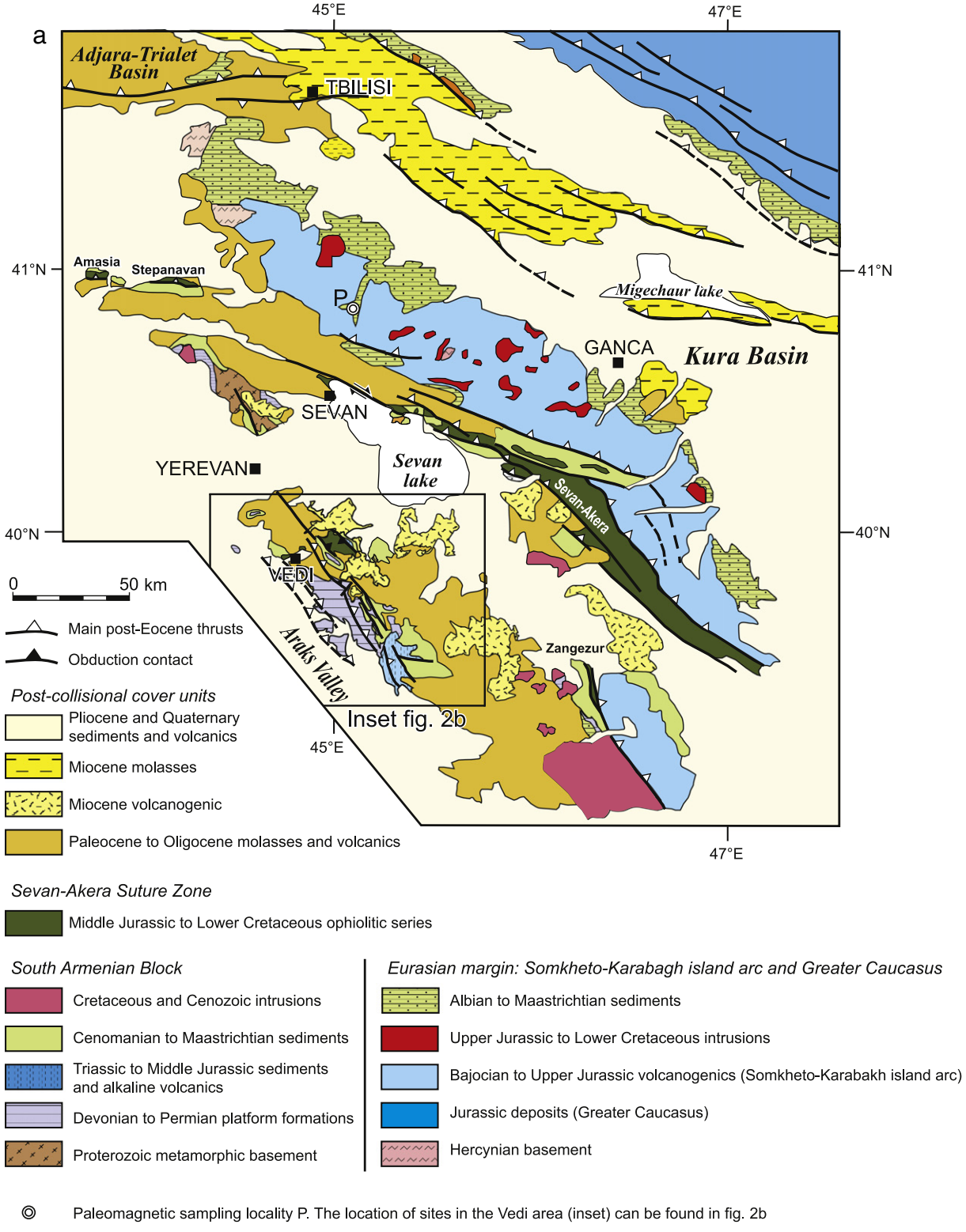

Fig. 2. a) Structural map of the Lesser Caucasus modified from Nalivkin (1976) and Sosson et al. (2010) including our sampling locations. Rectangle is the zoomed area in b). Note that the geologic information is generalized and that ages of the sampled rocks are not always in agreement with the age on the map (locality P-combined was sampled in upper Cretaceous rocks, whereas they were seemingly sampled in Jurassic rocks according to the map). b) Structural map of the Vedi area showing the relative positions of the sampling locations in the region after Sosson et al. (2010).

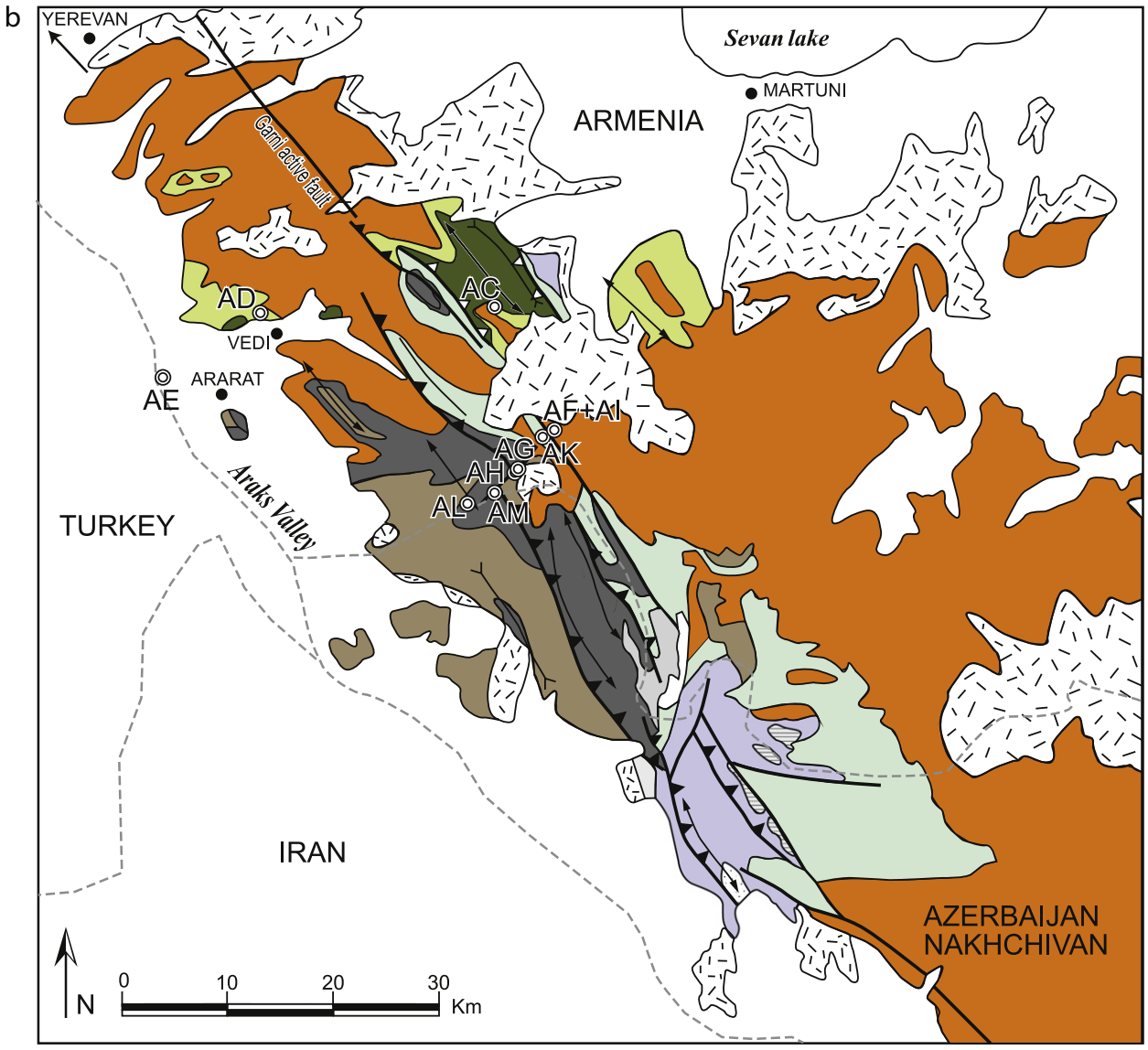

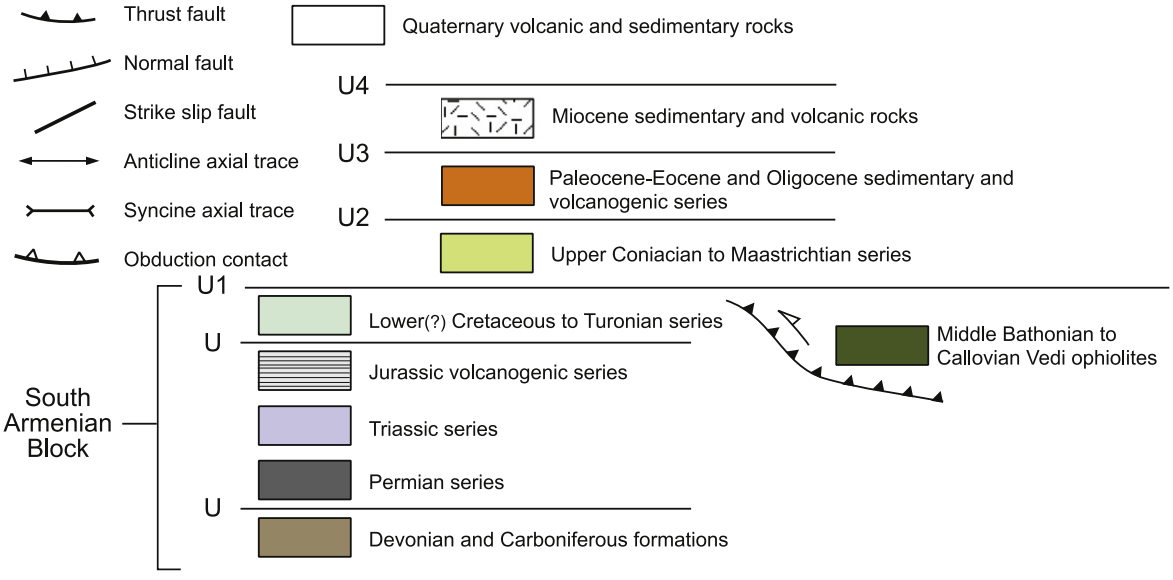

Fig. 2 (*continued*).

2. Geology of the South Armenian Block (SAB)

The SAB is part of the Lesser Caucasus and is well exposed in Armenia (Fig. 1). Its rifting history is very poorly known due to the absence of clear geologic evidence for rifting and is estimated to have occurred after the Early Jurassic, based on a paleomagnetic study by Bazhenov et al. (1996). In contrast to the Caledonian–Variscan Eurasian basement (Adamia, 1984; Adamia et al., 1983; Zakariadze et al., 1998), the SAB has a Proterozoic metamorphic basement of Gondwana affinity (Aghamalyan, 1978, 1998; Belov and Sokolov, 1973; Karyakin, 1989; Knipper and Khain, 1980; Knipper et al., 1986). The SAB is separated by the Sevan–Akera suture zone from the former southern Eurasian margin (Fig. 2a). To the east, it is bounded by the Iranian terranes. The southern boundary of the SAB is defined by the Bitlis–Zagros suture zone (Fig. 1) and to the west of the SAB is the Turkish Anatolide–Tauride Block (ATB). Estimated rifting initiation ages of the ATB from the African margin vary from Late Permian to Late Triassic (e.g. Moix et al., 2008; Robertson et al., 2004; Şengör and Yilmaz, 1981; Stampfli and Borel, 2002). The SAB and the ATB have often been described as two terranes. There are however several reasons to assume that the SAB is the eastern continuation of the ATB and represents the continental part of the Anatolide–Tauride–South Armenian (ATA) microplate (Barrier and Vrielynck, 2008; Okay and Tüysüz, 1999; Rolland et al., 2012). First, the SAB and ATB both have a basement of Gondwana origin. Second, the SAB and ATB have a similar position with respect to surrounding suture zones: the Izmir–Ankara–Erzincan suture zone (IAES, Fig. 1) and its eastern extension (the Amassia–Sevan–Akera suture zone; Fig. 2a) to the north and the Bitlis–Zagros suture zone to the south. Last, there is no clear geologic boundary between the ATB and SAB that would have potentially juxtaposed the two blocks (e.g. an ophiolite marking a former subduction zone or a large-scale lithospheric strike-slip fault). Therefore, a common rifting-history of ATA is likely.

The metamorphic basement of the SAB mainly consists of gneisses, micaschists and leucogranite intrusions (Aghamalyan, 1998; Hässig et al., 2014) and is overlain by unmetamorphosed Paleozoic sedimentary rocks (Karyakin, 1989; Paffenholtz, 1959). Paleozoic strata include Upper Devonian (Frasnian–Famennian) quartzites, sandstones and argillites, overlain by Lower Carboniferous reef limestones. The Early Carboniferous is overlain by Permian platform type limestones and marls and Triassic limestones that grade upward into Upper Triassic detrital deposits (Abramyan, 1951; Grigoryan, 1990). The contact between the Paleozoic deposits and the basement is not exposed. Siltstones of Bathonian age overlain by Callovian limestones are exposed 20 km to the south of Yeghegnadzor (Mandalyan, 1990). Exposures of Jurassic sequences are located in Nakhchivan (Azerbaijan) and in Iran where a 500 m-thick Lower and Middle Jurassic sedimentary sequence overlies Upper Triassic strata. Lower Cretaceous deposits are absent on the SAB and the Triassic–Jurassic deposits are unconformably overlain by Cenomanian reefal limestones that are covered by marls (Danelian et al., 2014; Eghoyan, 1955; Hakobyan, 1978; Paffenholtz, 1959; Sokolov, 1977). In the main area of our paleomagnetic study around the town of Vedi, the Cenomanian limestones are overlain by Upper Cenomanian flysch (Sosson et al., 2010) and Upper Coniacian to Santonian olistostromes that formed in front of the obducted ophiolitic nappes.

The entire Upper Devonian to early Late Cretaceous (Santonian) series covering the basement of the SAB is overlain by an ophiolite sequence of Middle to Late Jurassic age (178–155 Ma; radiolarian ages by Danelian et al. (2008, 2010, 2012) and Asatryan et al. (2012); $^{40}Ar/^{39}Ar$ ages by Galoyan et al. (2009), Rolland et al. (2010) and Hässig et al. (2013)). The ophiolite sequence is unconformably overlain by oceanic island basalts (OIBs) and arc-type volcanics (Galoyan, 2008; Galoyan et al., 2007, 2009) of Early Cretaceous age (Asatryan et al., 2012; Belov et al., 1991; Rolland et al., 2009b; Rolland et al., 2011), evidencing intra-oceanic plume and arc volcanism. The ophiolites, OIBs and arc-type volcanics are unconformably covered by Upper Coniacian to Santonian sedimentary strata (Sosson et al., 2010). These transgressive sedimentary rocks pass from conglomerates (that partially rework the underlying sequences) to reefal limestones, siltstones and pink pelagic clay-rich thin-bedded limestones. In the Vedi area, Campanian and Maastrichtian deposits are limited.

In the area of the Sevan–Akera suture zone Paleocene deposits are practically absent, probably as a result of erosion, whereas southward thick Paleocene molasse deposits unconformably overlie the ophiolitic sequence in the Vedi area. Unconformable atop the Paleocene deposits, late Middle Eocene and Oligocene deposits on the SAB comprise sedimentary and volcanogenic series. These are in turn disconformably overlain by Miocene sedimentary and volcanic rocks (Sosson et al., 2010).

The Eurasian foreland of the SAB is exposed in an orocline (Bazhenov and Burtman, 2002) that covers the entire Lesser Caucasus. From west to east, this northward convex orocline extends from the eastern Pontides in easternmost Turkey, to the Lesser Caucasus in Georgia and Armenia, and to the western part of Azerbaijan (see Fig. 1). The volcano-sedimentary cover of the eastern Pontides and the Lesser Caucasus rests on top of a Variscan basement (Adamia et al., 2011; Topuz et al., 2010). Rotations associated with orocline formation have been identified in Cretaceous and Eocene rocks (Bazhenov and Burtman, 2002). Timing of orocline formation is unknown due to a lack of paleomagnetic data from younger rocks.

3. Paleomagnetic sampling and methods

3.1. Paleomagnetic sampling

We sampled ten sites (mostly limestones) from the sedimentary cover of the SAB in the Vedi–Yeghegnadzor area (Fig. 2a–b; see GPS coordinates and description in Table 1). These include nine sampling sites on the SAB in Famennian (one), Tournaisian (two), Permian (two) and Cretaceous (three) rocks. One site covers the Permian–Triassic boundary. No Jurassic and Lower Cretaceous rocks were sampled because of the absence of exposed rocks suitable for paleomagnetism of this age in the Vedi–Yeghegnadzor area. Furthermore we sampled one Cretaceous locality (P in Fig. 2a), consisting of six sites (P-combined in Table 1) plus two individual sites (P5 and P7 in Table 1, represented by P on the map in Fig. 2a) in Eurasian margin sedimentary rocks ~35 km north of the city of Sevan (Fig. 2a). Wherever possible, we sampled strata with different bedding orientations in order to perform a fold test (P_combined, AD and AM). In total 757 individual paleomagnetic samples (i.e. cores) were collected. Samples were drilled using a motor drill and oriented with a magnetic compass. Sample orientations and bedding planes were corrected for the present-day declination of ~5.5°E. For NRM demagnetization measurements, samples were cut into standard size specimens (2.54 cm diameter, 2.2 cm height). The number of cores sampled per site is indicated in Table 1, as well as the number of demagnetized individual specimens per site.

Ages of the Paleozoic and lowermost Triassic rocks are based on conodont content, chondrichthye teeth and brachiopoda (Abramyan, 1951; Arakelyan, 1950, 1964; Ginter et al., 2011 and Grigoryan et al., 2012). Ages assigned to the Cretaceous rocks are based on nannoplankton content. To compare our results to the latitude versus age curves derived from the apparent polar wander (APW) path we derived numerical ages for Paleozoic and Triassic sampling sites following the time scale of Menning et al. (2006). For the Cretaceous and younger sites we correlated the nannoplankton zones to the time scales of Ogg et al. (2004) and Luterbacher et al. (2004).

3.2. Methods

Out of the 757 collected cores we demagnetized 766 specimens using alternating field (332 specimens) and thermal (434 specimens)

Table 1
Overview of all paleomagnetic results. Site, Rock type, Age (stage), Site lat. = site latitude, Site long. = site longitude, Age (numerical, from Ogg et al. (2008) for the Mesozoic sites and from Menning et al. (2006) for the Paleozoic sites), ΔAge = age error, N_{samp} = number of cores sampled, N_{af} = number of specimens demagnetized using AF demagnetization, N_{th} = number of specimens demagnetized using thermal demagnetization, N_{gc} = number of ChRM directions determined with great-circles, N/N_{45} = number of specimens of which a ChRM direction was determined/number of specimens remaining after the application of a fixed 45° cut-off on the VGPs, DEC = mean declination, ΔD_x = declination error determined from the A95 of the poles, INC = mean inclination, ΔI_x = inclination error determined from the A95 of the poles, k = precision parameter and α_{95} = cone of the 95% confidence limit for the ChRM directions, K = precision parameter and A95 = cone of confidence of the mean VGP, λ = paleolatitude of the site.
TK03 = results from the E/I model of Tauxe and Kent (2004) for sites AK, AD and P after applying a fixed 45° cut-off (AK_{45}, AD_{45}, P_{45}) on the datasets. INC− and INC+ is the 95% bootstrap error range of the most frequent inclination (INC) resulting from 5000 bootstraps. Corresponding paleolatitude ranges (PALAT) are calculated from the inclinations.

											In situ		
Site	Rock type	Age	Site lat.	Site long.	Age	ΔAge	N_{samp}	N_{af}	N_{th}	N_{gc}	N/N_{45}	DEC	ΔD_x
Eurasian margin													
P1	White clayey limestones	As for P3	40.85629	45.07150	80.3	3.3	5	0	4	0	4/4	13.9	10.2
P1A	White clayey limestones	As for P3	40.85344	45.08019	80.3	3.3	22	32	6	0	31/31	17.7	2.4
P2	White clayey limestones	As for P3	40.85438	45.08026	80.3	3.3	25	21	12	0	31/31	20.8	3.5
P3	White clayey limestones	Lower Campanian[a]	40.85202	45.08136	80.3	3.3	28	21	14	0	21/21	22.4	3.1
P4	White clayey limestones	Campanian[a]	40.85062	45.11193	80.3	3.3	27	28	16	0	42/42	186.0	2.9
P6	White clayey limestones	As for P3	40.84746	45.11780	80.3	3.3	18	13	11	0	21/21	17.6	4.5
P_combined	White clayey limestones	As for P3	40.85	45.10	80.3	3.3	125	115	63	0	150/150	15.9	1.7
P5	Volcano-sedimentary rocks	Coniacian	40.91843	45.15689	88.1	1.8	5	0	4	0	4/4	8.5	16.3
P7	White clayey limestones	Santonian–Maastrichtian	40.62531	44.92258	76.2	10.2	6	0	5	0	5/5	49.9	36.3
South Armenian Block													
AD	Pink clayey limestones	Santonian[a]	39.94797	44.69603	85.0	1.4	138	8	168	0	114/113	55.9	2.8
AK	Pink clayey limestones	Santonian[a]	39.83795	45.04678	85.0	1.4	102	3	106	0	105/105	66.9	2.0
AC	Gray clayey fine sandstones	Cenomanian[a]	39.96169	44.94235	96.6	3.0	34	22	10	0	30/30	62.0	37.9
AG	Gray limestones	Sakmarian (?)[b]	39.81381	44.97813	287.0	3.0	29	18	0	6	18/18	126.9	13.4
AF + AI	Red and gray (marly) limestones	Changhsingian–Indian (P–T boundary)[b]	39.84192	45.05039	251.0	0.0	93	26	15	0	36/33	66.0	3.8
AM	Gray limestones	Lower Permian	39.79054	44.95198	284.3	11.8	27	21	0	0	12/12	41.1	12.0
											5/5	3.6	45.4
AE	Gray limestones	Lower Tournaisian[b]	39.87936	44.57272	351.8	6.3	34	12	0	0	12/12	33.1	4.2
AH	Gray limestones	Lower (?) Tournaisian[b]	39.81284	44.97544	351.8	6.3	23	6	0	4	12/12	166.6	11.1
AL	Black nodulous limestones	Famennian[b]	39.80977	44.97224	365.8	7.8	16	15	0	0	15/15	252.3	99.9
						Total:	757	361	434				

TK03	Age	ΔAge	N	INC−	INC	INC+	PALAT	f
AD_{45}	85.0	1.4	112	46.7	51.2	61.8	27.9 < 31.9 < 43.0	0.93
AK_{45}	85.0	1.4	105	43.8	53.8	67.2	25.6 < 34.3 < 49.9	0.61
P_{45}[c]	80.3	3.3	129	48.5	55.6	65.9	29.5 < 36.1 < 48.2	0.75

[a] Dated on the basis of nannoplankton content. Because of the close proximity of sites P1, P1a, P2, P4 and P6 all sites were assigned a lower Campanian age.
[b] Dated on the basis of conodonts, chondrichthye teeth and/or brachiopoda.
[c] For reasons discussed in the text and in the supplementary data, site P6 was not taken int account for correction of inclination shallowing with the E/I method.

progressive stepwise demagnetization treatments (Table 1). Prior to alternating field (AF) demagnetization, all samples were heated up to 150 °C to 1) remove a viscous remanent magnetization (VRM) component, 2) remove possible stress in magnetite grains caused by surface oxidation at low temperatures (Gong et al., 2008; Van Velzen and Zijderveld, 1995) and 3) demagnetize goethite (often carrying the VRM). Thermal demagnetization of the NRM was measured on 2G DC SQUID cryogenic magnetometers at Utrecht University, the Netherlands (noise level 3×10^{-12} Am^2) and at Ludwig-Maximilians-Universität (LMU) Munich, Germany (noise level 10^{-12} Am^2). AF demagnetization was carried out on the in-house developed robotized magnetometer (noise level 10^{-12} Am^2) at Utrecht University. Demagnetization of the NRM is displayed in orthogonal vector diagrams (Zijderveld, 1967) in Fig. 3. Characteristic remanent magnetization (ChRM) directions were determined using principal component analysis (Kirschvink, 1980). For most specimens, five to seven successive demagnetization steps were included for the calculation of the ChRM direction.

To determine the magnetic mineralogy of the rocks, two types of thermomagnetic curves were obtained. For Santonian samples from sites AD and AK, the susceptibility versus temperature (K/T) was monitored in a 0.38 mT field on an Agico KLY-3S Kappabridge, equipped with a CS-L low temperature device and a CS-3 Furnace Apparatus at the University of Montpellier II, France. The powdered samples were sieved into 0.125 to 0.8 mm grain sizes. They were first heated from liquid Nitrogen to room temperature, then heated and cooled in air or/and in argon up to successively 200, 350, 500, 600 and 700 °C to determine the temperature at which possible chemical changes occur. At the end of this cycle, a low temperature heating run was performed again on the same powder. For the Campanian rocks of locality P-combined, the thermomagnetic curves were performed in high field (~500 mT) using a variable field translation balance (VFTB, Petersen Instruments, LMU Munich; Krasa et al., 2007). All rock magnetic results are presented in Fig. 4.

At the Institute for Rock Magnetism (University of Minnesota, USA), low temperature experiments were carried out on subsamples (~0.5 g rock chips) of paleomagnetic cores from sites AD and AK on a Quantum Designs Magnetic Property Measurement System (MPMS) cryogenic magnetometer (sensitivity 10^{-10} Am^2). Prior to measurements in the MPMS, the subsamples were given a 2.5 T isothermal remanent magnetization (IRM) to optimize centering of the subsample with respect to the superconducting quantum interference device (SQUID), except for one subsample of AK06 (Fig. 4l) that was heated at 150 °C prior to the experiment to demagnetize goetithe. In a Field Cooled–Zero Field Cooled (FC-ZFC) experiment, subsamples were cooled from room temperature (RT) to 20 K, first in a 2.5 T field and then in zero field (ZF), and given a 2.5 T isothermal remanent magnetization (IRM) at 20 K. The magnetization was measured on warming to room temperature in zero field (Fig. 4j). Following this step, a room temperature saturation isothermal remanent magnetization (RTSIRM) experiment was carried out, after imparting a 2.5 T IRM on each subsample at room temperature. Measurements of the magnetization were obtained upon cooling

						Tilt corrected								
INC	ΔI_x	k	α_{95}	K	A_{95}	N/N_{45}	DEC	ΔD_x	INC	ΔI_x	λ	k	α_{95}	K	A_{95}
21.3	18.0	44.9	13.9	85.8	10.0	4/4	19.7	12.1	38.7	15.8	21.8	44.9	13.9	68.2	11.2
14.3	4.6	77.8	2.9	117.9	2.4	31/31	24.3	3.5	43.8	4.1	25.6	77.8	2.9	65.4	3.2
16.0	6.6	43.0	4.0	55.3	3.5	31/31	26.3	5.0	46.1	5.4	27.5	43.3	4.0	35.6	4.4
17.7	5.8	70.4	3.8	106.0	3.1	21/21	29.4	4.6	49.9	4.5	30.7	82.3	3.5	65.0	4.0
−29.8	4.5	37.3	3.7	65.7	2.7	42/42	198.2	3.6	−52.4	3.2	33.0	71.0	2.6	55.4	3.0
30.2	7.1	43.3	4.9	54.2	4.4	21/21	8.5	6.4	45.7	7.0	27.2	39.9	5.1	32.0	5.7
22.0	3.1	30.9	2.1	46.2	1.7	150/150	21.5	2.2	47.9	2.2	28.9	46.7	1.7	37.6	1.9
48.7	16.3	74.0	10.7	43.2	14.1	4/4	192.9	15.0	46.2	16.2	27.6	74.0	10.7	48.6	13.3
62.5	20.7	21.5	16.9	10.1	25.2	5/5	2.3	58.0	72.0	17.7	57.0	21.5	16.9	8.7	27.5
28.4	4.5	22.3	2.9	25.3	2.7	114/112	63.6	3.1	47.1	3.2	28.3	31.8	2.4	25.7	2.7
10.3	3.9	38.0	2.3	49.8	2.0	105/105	74.8	2.3	42.0	2.8	24.2	45.4	2.1	42.4	2.1
85.6	2.7	87.5	2.8	25.2	5.3	30/30	52.0	3.9	50.7	3.6	31.4	87.5	2.8	62.6	3.3
78.5	2.8	153.6	2.8	49.0	5.0	18/18	77.0	4.9	51.8	4.4	32.5	117.9	3.2	71.4	4.1
5.3	7.5	28.4	4.8	44.4	3.8	36/33	35.8	35.0	82.3	4.5	74.9	28.2	4.8	9.3	8.6
33.3	17.6	14.5	11.8	15.5	11.4	17/14	105.2	19.7	−69.9	7.8	53.7	30.0	7.4	12.9	11.5
−70.9	15.8	30.9	14.0	11.2	23.9										
45.0	4.7	144.3	3.6	131.7	3.8	12/12	42.7	3.1	17.1	5.8	8.7	93.5	4.5	196.2	3.1
56.4	8.5	32.9	7.7	25.2	8.8	12/12	118.1	6.1	48.0	6.2	29.1	99.7	4.4	67.4	5.3
88.9	3.4	118.3	3.5	32.8	6.8	15/15	68.0	4.4	52.5	3.9	33.1	118.3	3.5	106.5	3.7

to 20 K and subsequent warming to 300 K, both in zero field. The NRM upon cooling and warming in zero field from room temperature down to 20 K was measured on a number of subsamples. An example is given in Fig. 4l (AK06).

Site mean directions (Fig. 5) were calculated from the individual ChRM directions using Fisher (1953) statistics. The virtual geomagnetic poles (VGPs) corresponding to each individual ChRM direction were also calculated. For sites AD, AK and locality P-combined they are displayed in Fig. 7. On each site a fixed 45° cut-off was applied to the VGPs to remove outliers. The errors in declination (ΔD_x) and inclination (ΔI_x) are calculated from the A95 (95% confidence angle on the mean VGP) following Butler (1992). Because the directional distributions become more elongated toward lower latitudes (Creer et al., 1959; Deenen et al., 2011; Tauxe and Kent, 2004; Tauxe et al., 2008), this approach more realistically describes the associated errors.

Sites AH and AG contain specimens (four and six respectively) that yield NRM directions that are intermediate between two overlapping temperature or coercivity components. To determine the ChRM directions for these specimens we used the great circle approach of McFadden and McElhinny (1988). This method determines the direction that lies closest on the great circle to the average direction from well-determined ChRM directions. The great circles are indicated in Fig. 5n and r. The bedding orientation of the outcrops at sites AM, AD and three sites of locality P-combined (P3, P4, P6) varies within ~10–100 meter scale, due to small-scale folding. Bedding orientation also varies between the individual sites sampled at locality P-combined (sampled up to ~4 km apart). This allowed us to carry out fold tests on AM, AD and locality P-combined (Fig. 6; Tauxe and Watson, 1994). Fold tests were carried out following two different procedures: (1) by using all individual ChRM directions and their corresponding bedding planes, and (2) by using the mean ChRM direction of all the specimens that were taken from layers with the same bedding plane orientation. This last procedure gives equal weight to each different bedding plane orientation, disregarding the number of samples in each group. In both cases, however, the results of the fold test are very similar.

On locality P-combined we carried out the reversal test of McFadden and McElhinny (1990) and their classification (A, B, C, indeterminate) based on their critical angle γ_c and the angle γ between the means. The program uses Monte Carlo simulation, thereby effectively applying the (Watson, 1983) V_w statistic test.

All samples in this study were collected from sedimentary rocks. Paleomagnetic data from sedimentary rocks can be corrected for the paleohorizontal and can properly average out secular variation of the Earth's magnetic field, providing the sampled stratigraphic succession covers sufficient time, i.e. ~10 kyr (when encountering an excursion interval, this may well be >100 kyr; Merrill and McFadden, 2003). Contrary to igneous rocks, data from sedimentary rocks are notably prone to inclination shallowing, which leads to an underestimation of paleolatitude. Inclination shallowing has been recognized for decades and resulted in numerous studies examining how rocks acquire their remanence, studying the effects of dewatering and compaction on sediments during burial and developing methods that correct for inclination shallowing. Inclination shallowing in marine carbonates, however, is not always identified — potentially due to the effect of delayed acquisition of remanence (Van Hoof and Langereis, 1991), after dewatering and compaction. Nevertheless, Celaya and Clement (1988) showed unequivocal evidence for inclination shallowing in Deep Sea Drilling Project (DSDP) cores with Miocene to recent sediments from the North Atlantic. In this particular study, inclination shallowing was only observed in sediments with a carbonate content >80% and the magnitude of shallowing increased with core depth as a result of compaction. An overview of additional studies that recognized inclination shallowing in carbonates can be found in Kodama (2012). The overview includes a variety of sediments such as carbonate

concretions within North American Upper Cretaceous rocks (Kim and Kodama, 2004), Carboniferous and Jurassic–Cretaceous marine limestones in the Donbas region (Meijers et al., 2010a) and the circum-Black Sea region (Meijers et al., 2010b,c), and DSDP limestone samples from the Pacific plate (Hodych and Bijaksana, 1993). The study on DSDP cores by Hodych and Bijaksana (1993) concludes that inclination shallowing is likely caused by compaction, similar to the conclusions of Celaya and Clement (1988).

Inclination shallowing in detrital sedimentary rocks is widely observed and has been extensively studied in depositional experiments (e.g. Bilardello, 2013; Tan et al., 2002; Tauxe and Kent, 1984). Depositional processes on detrital sediments can be simulated in a laboratory environment to some extent, but simulating carbonate precipitation is very challenging and therefore complicates understanding the potential influence of depositional processes on inclination shallowing in limestones. For our understanding of depositional effects on inclination shallowing in carbonates, we therefore have to rely on studies performed on detrital sediments. Compaction experiments by Anson and Kodama (1987) on acicular and equi-dimensional magnetite led to the hypothesis that shallowing resulted from magnetite particles sticking to clay particles by electrostatic attraction. This forces the magnetite particles to rotate with the clay particles during loading of the sediment. This hypothesis was confirmed by SEM inspection in a study by Sun and Kodama (1992) that furthermore pointed out the importance of clay content: the flattening factor decreases (i.e. inclination shallowing increases) with increasing clay content. This could be important for this study. The marine carbonates to which we apply an inclination shallowing correction are clay-rich limestones.

Approaches used to correct for inclination shallowing are based on various rock magnetic and statistical parameters (Jackson et al., 1991; Tan and Kodama, 2003; Tauxe and Kent, 2004). We apply the statistical elongation/inclination (E/I) method of Tauxe et al. (2008) to correct for inclination shallowing. This model is based on the TK03.GAD field model, which in turn is based on the assumption that the Earth's magnetic field averaged over a time interval long enough to average out the secular variation resembles that of a geocentric axial dipole (GAD). Because the E/I method analyzes the distribution of individual directions, it requires a large data set as input (with N typically >100). Therefore, we could only apply this method to three data sets, namely sites AD, AK and locality P-combined (Fig. 7).

4. Results

Initial intensities at 20 °C range from 200 to 7000 μA/m for sites P, AI, AF, AC, AD and AK. Sites that were thermally demagnetized up to 150 °C prior to AF demagnetization yield initial intensities ranging between 200 and 5000 μA/m after the initial step of 150 °C (sites AL, AH, AG and AE). Site AM yields very low initial intensities of 10–70 μA/m (after 150 °C). The mean ChRMs before (nt) and after (tc) tilt correction are given in Table 1 and are displayed in Fig. 5. The presence of a high coercivity mineral, after initial thermal demagnetization at 150 °C, prevented full AF demagnetization of the NRM of specimens from sites AD and AK (e.g. Fig. 3k). Therefore we demagnetized nearly all specimens from sites AD and AK thermally. In our sampling process, we intended to correct all sampled sediments for inclination shallowing using the E/I method. We therefore sampled a relatively large number of cores per site/locality during the first field season. During a second field season we increased the number of cores, specifically for sites AD, AK and locality P-combined (for which we obtained good results), to allow running the statistical model.

4.1. Paleozoic sites — SAB sediments

Samples from six sites within the Paleozoic cover of the SAB were taken from the Vedi region (Fig. 2b). Rocks at most sampled Paleozoic limestone levels appear to be recrystallized. Only site AF + AI seemed to be partially recrystallized. We calculated the (tilt corrected) mean ChRM directions discussed below based on AF demagnetization, after the application of an initial thermal demagnetization step at 150 °C. Site AL (Famennian) consist of black nodular limestones with bivalves, and the ChRM directions were isolated between 10 mT and ~40 mT (Fig. 3s). One specimen yielded a reverse ChRM component. After correction for bedding tilt, the mean ChRM direction for this site (N = 15) is D = 68.0°, I = 52.5° (Fig. 5s; Table 1). Site AH – gray limestone (Tournaisian) – yields a mean ChRM direction of (N = 12) D = 118.1°, I = 48.0° (Fig. 5r, Table 1) that was isolated between 25 mT and ~65 mT (Fig. 3r). The ChRM directions of the other Tournaisian site AE – also gray limestones but intruded by sills of unknown age – were typically isolated between 15 mT and ~80 mT (Fig. 3q) and the mean for this site (N = 12) is D = 42.7°, I = 17.1° (Fig. 5q, Table 1). Samples from site AM, presumably of Permian age, were taken from gray limestones. The sampling site consists of two parts with different bedding orientations. The structural relation between the two parts is not obvious in the field (i.e. faulting versus folding). The ChRM was typically isolated between 5 mT and ~50 mT (Fig. 3p). Before tilt correction, there are two distinct groups with different ChRM directions (Fig. 5p). Tilt correction of the individual ChRM directions and a fold test lead us to conclude that the southernmost, south-dipping part must be overturned. Site AM passes both fold tests that were carried out (Fig. 6i and r) and after tilt correction the mean ChRM direction (N = 14) is D = 105.2°, I = −69.9° (Fig. 5p, Table 1). Site AF + AI is a section through the Permo-Triassic boundary (site AF refers to the Permian interval and site AI to the Triassic interval). The samples from site AF consist of gray limestones and those from site AI of gray and pink (marly) limestones. In total, 41 specimens were demagnetized, 26 using AF demagnetization and 15 using thermal demagnetization (Fig. 3o). The mean ChRM direction (N = 33) is D = 35.8°, I = 82.3° (Fig. 5o, Table 1). Site AG was sampled in gray limestones of Permian age and the ChRM was typically isolated between ~25 mT and ~60 mT (Fig. 3m). The mean ChRM after tilt correction (N = 18) is D = 77.0°, I = 51.8° (Fig. 5n, Table 1).

4.2. Cretaceous sites — Eurasian margin sediments

Samples from eight sites were taken from Eurasian margin sedimentary rocks north of Lake Sevan (P, Fig. 2a). Six of the eight sites (P1, P1A, P2, P3, P4 and P6) were taken in very close proximity to each other along an E–W profile of ~4 km on one mountain and within the same Lower Campanian succession. These clayey white pelagic limestones with beds of 1–30 cm thickness are intercalated with thin (mm-scale) layers of marl (Fig. 5j). Sites P5 and P7 were sampled in volcano-sedimentary rocks and white limestones of probably Late Cretaceous age. The ages of P5 (Coniacian) and P7 (Santonian–Maastrichtian) are deduced from the geologic map (Kharazian and Sargsyan, 2005; scale 1:500.000) and are therefore not considered very reliable.

Four specimens of site P5 were thermally demagnetized (Fig. 3d). The mean ChRM direction of site P5 before tilt correction is very close to the present-day geocentric axial dipole (GAD) field direction and the mean ChRM direction after tilt correction (N = 4) is D = 192.9°, I = 46.2° (Fig. 5h, Table 1), which would either imply a southern hemisphere position (paleolatitude of 27°S) at the time of deposition or a 180° post-deposition rotation. We render both scenarios unlikely, and conclude that the non-tilt corrected ChRM direction represents the present-day GAD field. Five specimens of site P7 were thermally demagnetized (Fig. 3g). The mean ChRM direction after tilt correction (N = 5) is D = 2.3°, I = 72.0° (Fig. 5i, Table 1). However, the results from this site were not further considered, because of the absence of reliable age constraints.

We combined the six sites (P1, P1A, P2, P3, P4 and P6) into locality P-combined. In total, 125 samples were taken from this locality. A total of 178 specimens were demagnetized, of which 63 using thermal

demagnetization and 115 using AF demagnetization. Typical demagnetization diagrams are shown in Fig. 3a–c and e–f. Approximately half of the specimens show a low temperature (~20°–200 °C) or low coercive force (5 mT–15 mT) component that represents a present-day GAD field overprint that could be sufficiently isolated (Fig. 8d). In the other half of the samples this component was likely present, but not retrievable due to the initial step of 150 °C. The high temperature/high coercive force component was typically isolated between 200°/300 °C and 480°/540 °C or 15 mT and 55 mT (after heating to 150 °C). Therefore the magnetic carrier of the ChRM is likely (Ti-poor) magnetite. This is supported by thermomagnetic curves ran in high field (0.5 T, Fig. 4o) and by hysteresis data (Fig. 4p). In some samples, however, the

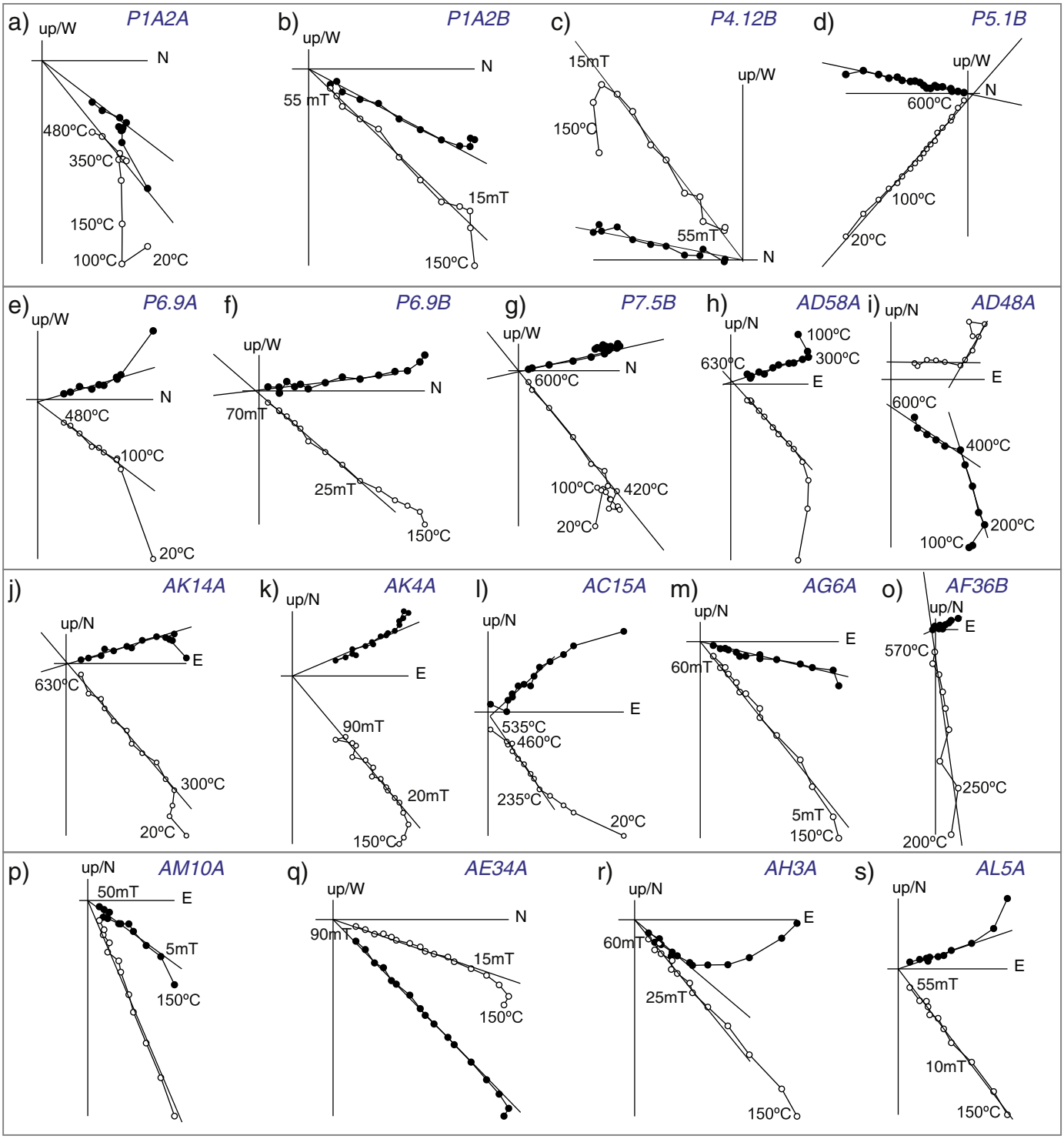

Fig. 3. a–s) Orthogonal vector diagrams (Zijderveld, 1967), showing characteristic demagnetization diagrams for the sampled sites. Closed (open) circles indicate the projection on the horizontal (vertical) plane. Alternating field and thermal demagnetization steps are indicated. All diagrams are displayed after bedding tilt correction. Examples of samples from which specimens were AF and thermally demagnetized are included for comparison of both techniques, see a–b) and e–f).

paramagnetic contribution may be dominant (Fig. 4q). All samples from site P4 carry a reverse polarity high temperature/high coercive force component (Fig. 5e), as well as two samples (three specimens) from site P2 (Fig. 5c) that are confined to the base of the sampled stratigraphic interval. Considering the geographic location of the sites and the overall bedding orientation, it is therefore very likely

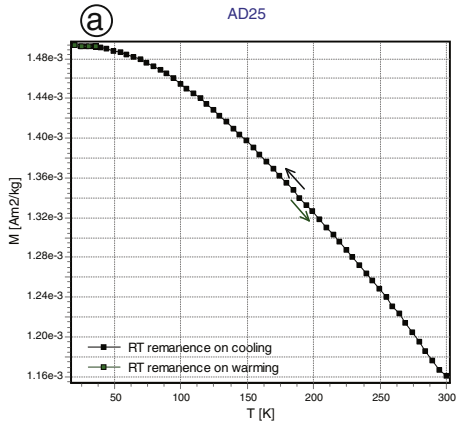

Thermal demag (300-20-300K) of Room Temperature (RT) SIRM (2.5T)

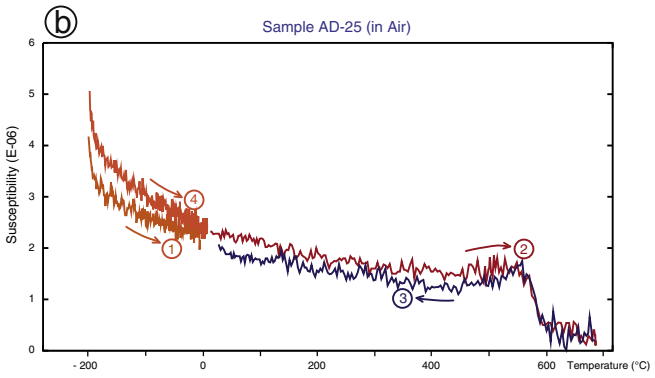

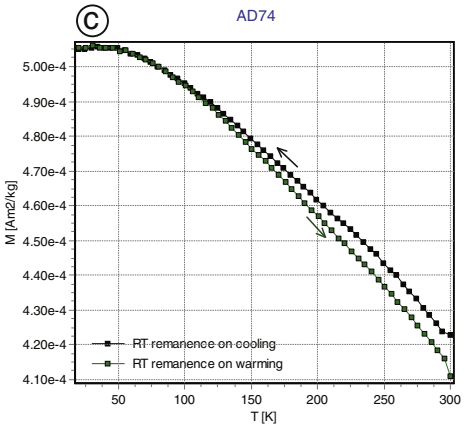

Thermal demag (300-20-300K) of Room Temperature (RT) SIRM (2.5T)

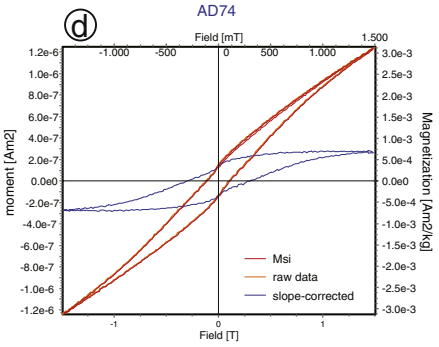

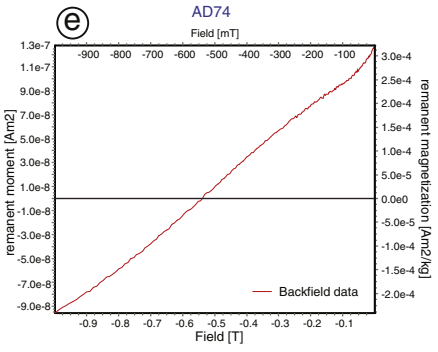

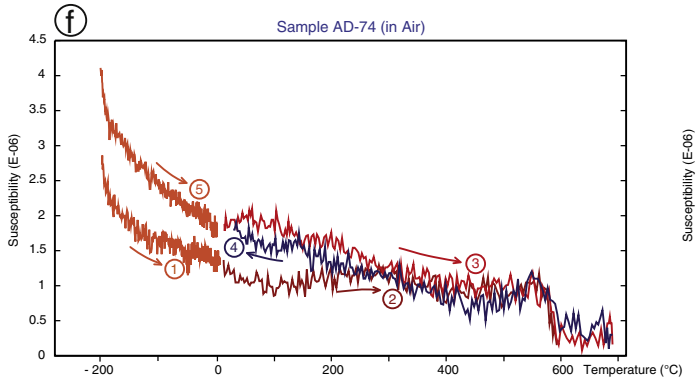

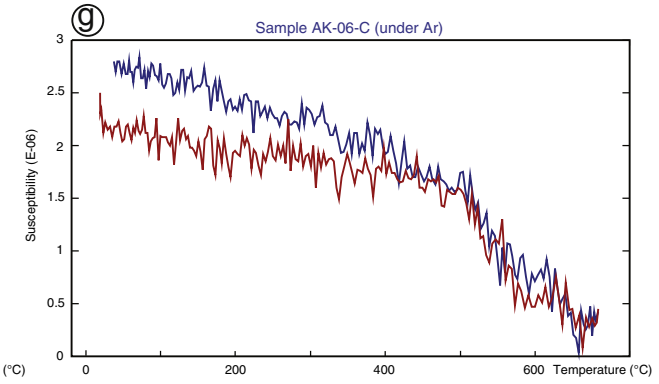

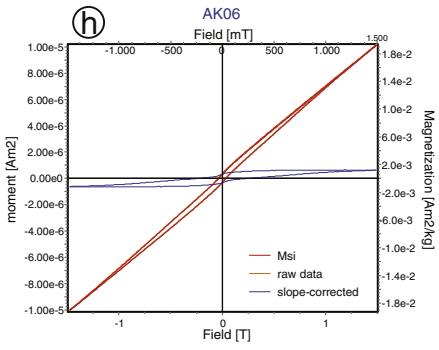

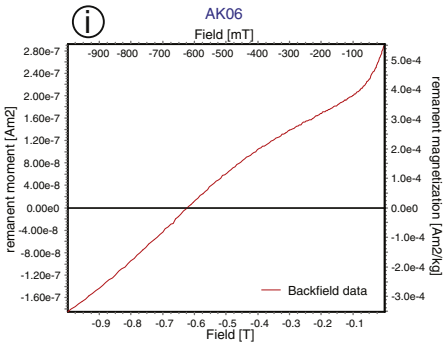

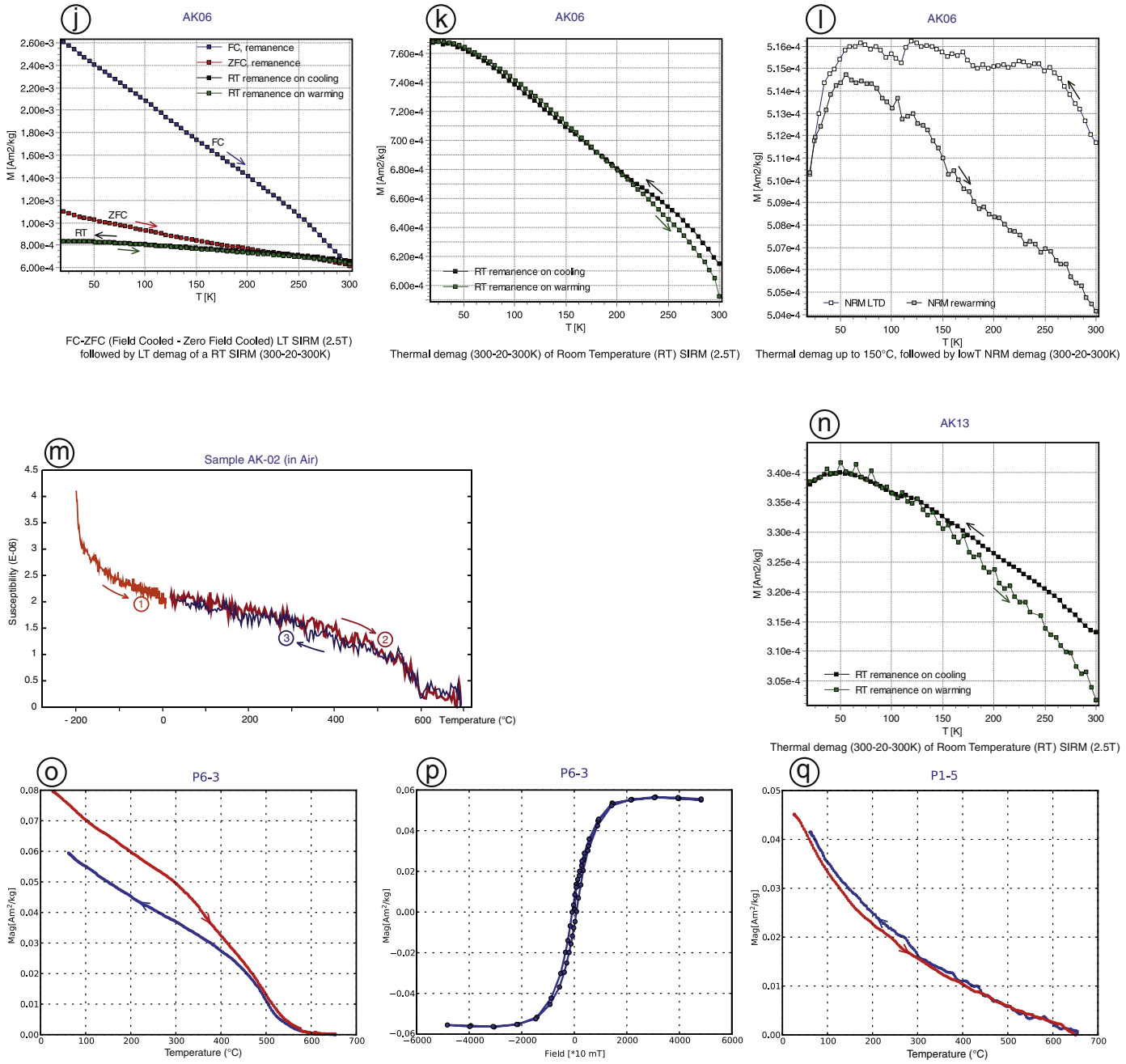

Fig. 4. Thermomagnetic and hysteresis properties of samples of Upper Cretaceous rocks from sites AD (a–f), AK (g–n) and P (o–q). b, f, g, m) Susceptibility as a function of temperature, from liquid nitrogen (−196 °C) to 700 °C, in air or in Argon; o, q) high field (0.5 T) thermomagnetic curves; d, h, p) hysteresis cycles (induced and remanent magnetizations); e and i) backfield determination of H_{rc}; a, c, k, n) low temperature variation (300–20 K–300 K) of a Room Temperature (RT) IRM acquired in 2.5 T; j) Field Cooled (FC) and Zero Field Cooled (ZFC) of an IRM acquired in 2.5 T at 20 K. The sample is first cooled in a 2.5 T field, then the remanence is measured upon heating (blue curve) followed by cooling in zero field. After reaching the minimum temperature (20 K) it is given an IRM of 2.5 T and the remanence is measured upon heating (red curve). The other two RT curves are duplicates of the experiment in k); l) low temperature demagnetization of a sample that was initially heated at 150 °C to demagnetize goethite. demag = demagnetization.

that the locality P-combined was sampled around the reversal transition from chron C33r to C33n (~80 Ma). All individual site mean directions can be found in Fig. 5a–f and Table 1. The site mean direction for locality P-combined (N = 150) after tilt correction is: D = 21.5°, I = 47.9° (Fig. 5g, Table 1).

The fold test on all individual ChRM directions (Fig. 6a–c) results in tightest clustering (95% bootstrap level) between 75% and 97% untilting while the fold test on the mean ChRM directions per individual bedding plane (Fig. 6j–l) gives the tightest clustering between 85% and 114%. The reversal test between the normal and reverse means is negative ($\gamma = 5.1° > \gamma_c = 3.6°$). Nevertheless, we interpret the high temperature/high coercive force component as a primary ChRM direction, based on the positive fold test. Correction for inclination shallowing on the full data set of P-combined with the E/I method (Tauxe et al., 2008), leads to a corrected inclination of (N = 150) I = 61.2° (with a 95% confidence interval (52.1, 73.4); see Supplementary data). This correction is significant. When examining the variation in ChRM directions of the individual sites that constitute locality P-combined more carefully, the declinations of P6 seem to be divided in two subgroups: one with a direction close to the mean ChRM direction for locality P-combined and one which has northern declinations. We therefore carried out a number of runs

omitting P-sites one-by-one in order to determine whether the results are robust (see Supplementary data). This resulted in a preferred E/I run that omits site P6, leading to the following results: N = 129, I = 48.5° < 55.6° < 65.9°. This correction of 7.5° is significant (Fig. 7n).

4.3. Cretaceous sites — SAB sediments

In the Vedi area we sampled three sites in Upper Cretaceous rocks from the SAB: sites AC, AD and AK. Site AC was sampled in gray clayey fine sandstones of Cenomanian age. The limited extent of the outcrop and its poor quality did not allow us to sample more than 34 cores. Ten specimens were demagnetized using thermal demagnetization (Fig. 3l). Twenty-two specimens were demagnetized using AF demagnetization. About half of the samples yield a low temperature/low coercive force component (ranging respectively 100 °C–200 °C and 150 °C–20 mT) that is statistically similar to the present-day GAD field at the sampling location (Fig. 8b). The mean ChRM direction that was isolated between 235 °C and 500 °C or 15 mT and 70 mT (after

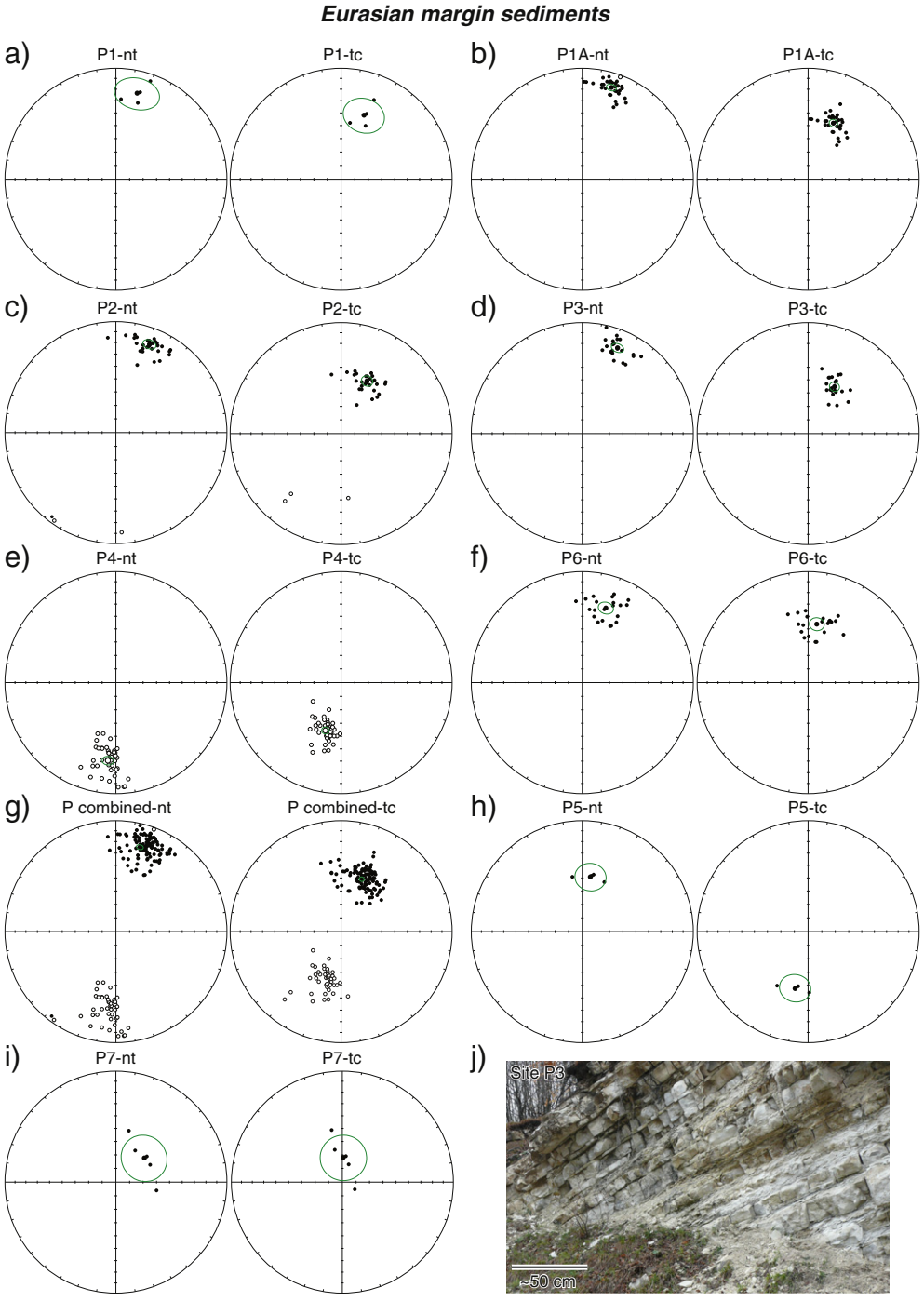

Fig. 5. a–i and k–s) Equal area projections of the ChRM directions of all sampled sites (Table 1). Open (closed) symbols denote projection on upper (lower) hemisphere. Large closed black circles surrounded by green circles indicate respectively the mean directions and their cone of confidence (α_{95}) before (nt) and after (tc) tilt correction. Red circles indicate the individual directions rejected after applying a 45° cut-off on the virtual geomagnetic poles. For site AH and AG, gray lines indicate the great circles that were used to calculate the best fitting ChRM directions, with the corresponding calculated directions in blue (McFadden and McElhinny, 1988). j and t) Pictures of representative parts of the outcrops of locality P-combined and site AK, respectively.

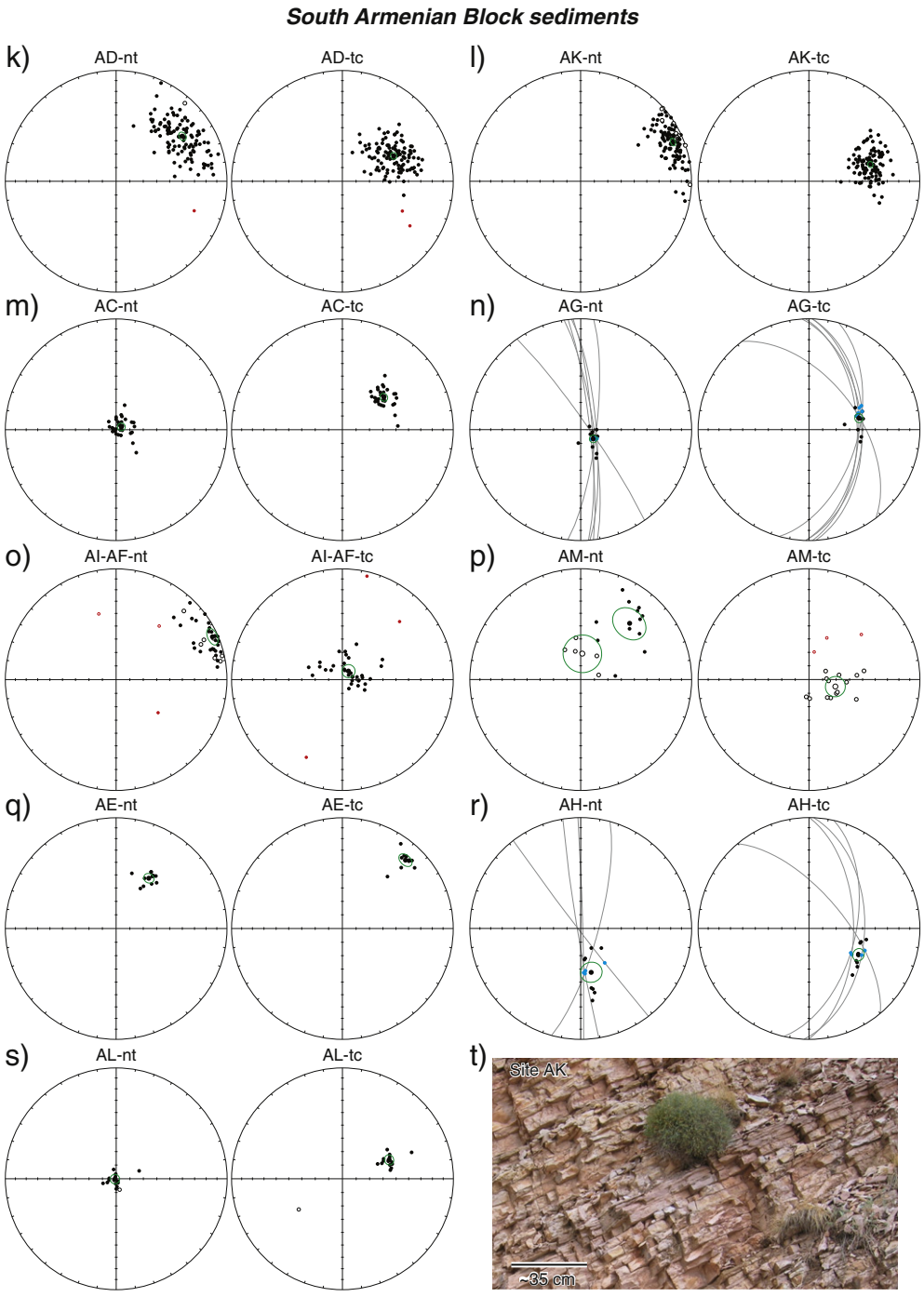

Fig. 5 (*continued*).

150 °C) after tilt correction (N = 30) is: D = 52.0° and I = 50.7° (Table 1, Fig. 5m).

Sites AK and AD were both sampled in pink pelagic limestones of Santonian age. The thin bedded (~1–10 cm), friable and clay-rich limestones alternate with thin (mm-scale) marl layers (see Fig. 5t). We collected 102 cores from site AK of which three specimens were demagnetized using AF demagnetization and 106 specimens were thermally demagnetized. Typical demagnetization diagrams for site AK can be found in Fig. 3j and k. Most samples from site AK yield a low temperature (~20 °C–200/250 °C) or low coercive force component (~150 °C–10 mT; Fig. 8a) that is possibly an intermediate direction between the present-day GAD field at the site location and the ChRM direction. The ChRM direction was isolated between ~200/250 °C and 570/600 °C. All samples yield normal polarity, which is in agreement with their deposition and magnetic acquisition during the Cretaceous Normal Superchron. The mean ChRM direction after tilt correction (N = 105) is D = 74.8°, I = 42.0° (Fig. 5l, Table 1). Within-site variation of bedding orientations is too low to carry out a reliable fold test. However, we note that the individual ChRM directions are slightly more tightly clustered after correction for bedding tilt (k_{tc} = 45.4) than before (k_{nt} = 38.0; see Table 1). Correction for inclination shallowing with the E/I method (Tauxe et al., 2008), leads to a

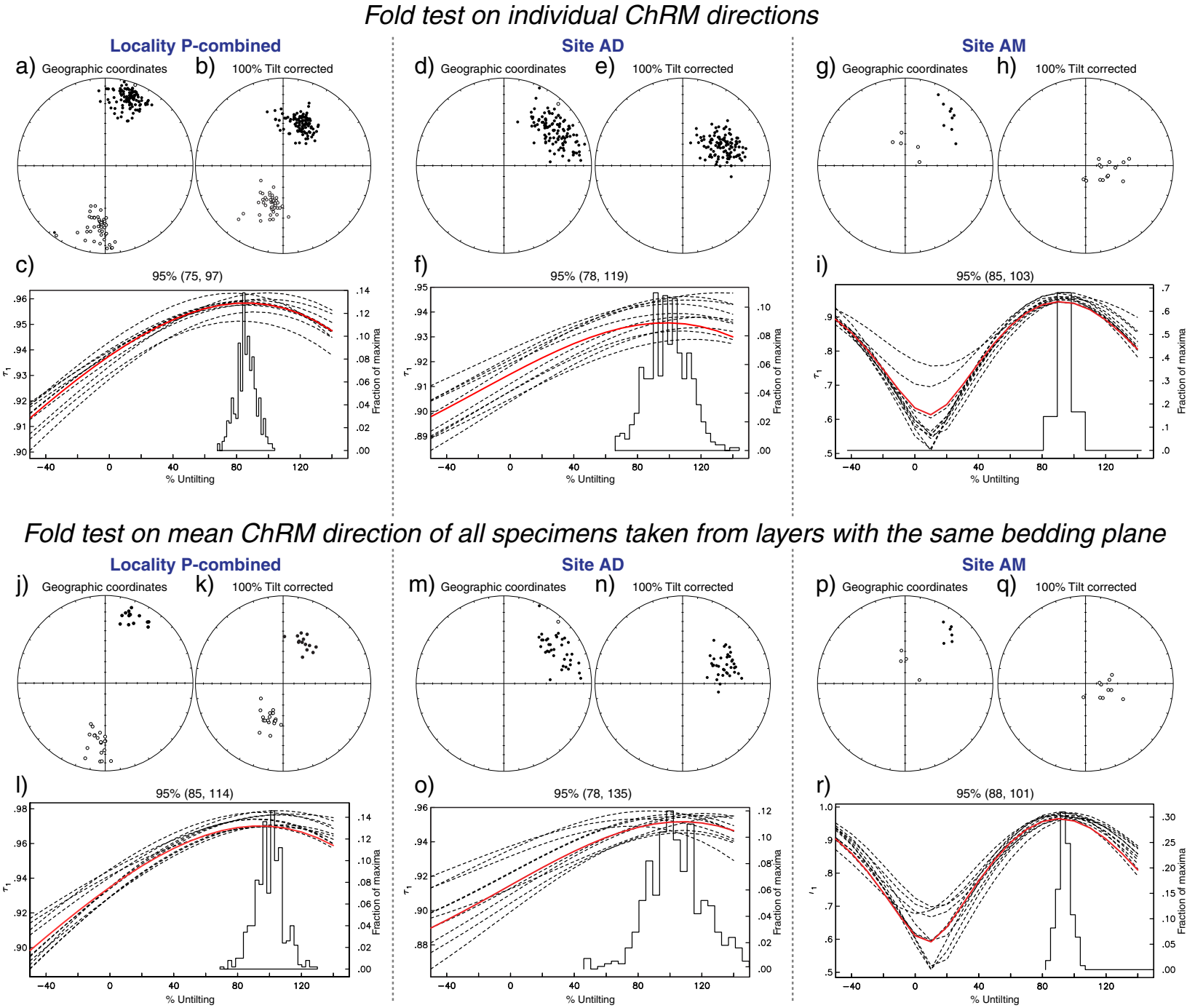
Fold test on individual ChRM directions
Locality P-combined
Site AD
Site AM
a) Geographic coordinates
b) 100% Tilt corrected
d) Geographic coordinates
e) 100% Tilt corrected
g) Geographic coordinates
h) 100% Tilt corrected
c)
95% (75, 97)
f)
95% (78, 119)
i)
95% (85, 103)
% Untilting
Fraction of maxima
Fold test on mean ChRM direction of all specimens taken from layers with the same bedding plane
Locality P-combined
Site AD
Site AM
j) Geographic coordinates
k) 100% Tilt corrected
m) Geographic coordinates
n) 100% Tilt corrected
p) Geographic coordinates
q) 100% Tilt corrected
l)
95% (85, 114)
o)
95% (78, 135)
r)
95% (88, 101)
% Untilting
Fraction of maxima

corrected inclination (N = 105) of I = 43.8° < 53.8° < 67.2° (Fig. 7r). This correction of ~12° is significant at the 95% confidence level of the bootstrap model.

From site AD, eight specimens were demagnetized using AF demagnetization and 168 specimens were thermally demagnetized. The demagnetization response can be divided in two groups: (1) specimens that yield a low temperature component (~20–250 °C) and a high temperature component (~250–600 °C) that defines a stable endpoint trajectory to the origin (Fig. 3h) and (2) a group of specimens that sometimes yield a low temperature component (~20–200 °C) plus a medium temperature component (~200–400 °C) and a high temperature component (~400–570 °C) that does not define a stable endpoint trajectory (Fig. 3i). This high temperature component cannot be demagnetized any further because of formation of new magnetic minerals at ~600 °C. The low temperature component in both groups of samples is close to the present-day GAD field at the sampling location (Fig. 8c). The high temperature component of the first group of samples that demagnetizes to the origin always yields a normal polarity. Similar to site AK, this normal polarity is expected for sediments that were deposited during the Cretaceous Normal Superchron. The mean ChRM direction for the first group of samples after tilt correction (N = 112) is D = 63.6°, I = 47.1° (Table 1, Fig. 5k). This mean ChRM direction is in relatively good agreement with the mean ChRM direction of nearby site AK. Using the high temperature ChRM directions, we carried out fold tests following the two different procedures described in the Methods section. Both fold tests are positive (Fig. 6d–f and m–o). Therefore, we interpret the high temperature component in the specimens from group one as a primary ChRM direction. Correction for inclination shallowing with the E/I method of this primary ChRM direction (Tauxe et al., 2008), leads to a corrected inclination (N = 112) of I = 46.7° < 51.2° < 61.8° (Fig. 7p). This correction of ~4° is (just) not significant at the level of the 95% bootstrap error of the model.

The medium and high temperatures components from the second group of samples are most likely secondary in origin and thus remagnetized. Both components, as well as the primary ChRM direction of the first group of samples, are plotted in Fig. 8e–f in in-situ and tilt corrected coordinates. The two great circles through all the individual medium (MT) and high temperature (HT) directions of samples from group 2 are also plotted in Fig. 8e–f. These great circles lie close to each other and the mean ChRM direction of the first group lies close to both great circles, notably after tilt correction. Therefore, we interpret the medium and high temperature components of group 2 as intermediate directions between a reverse polarity overprint and the primary normal ChRM direction. The origin of this reverse overprint is unknown. As can be seen in Fig. 8e, these secondary remagnetizations do not originate from a reverse pre-Brunhes GAD field (given that the paleolatitudinal motion and rotational history over the past ~1 Myr is negligible) because the two great circles do not include a reverse polarity GAD field direction (red open star in Fig. 8e).

The pink pelagic limestones of sites AK and AD have a complex magnetic mineralogy. All samples contain goethite, based on the increase in spontaneous magnetization between 300 K and 10 K in the room temperature (RT) saturation isothermal remanent magnetization (SIRM) curves (Fig. 4a, c, k, l and n), the large differences between the ZFC (Zero Field Cooled) curve and FC (Field Cooled) curve (Fig. 4j; Liu et al., 2006) and an up to ~50% intensity drop of the NRM after heating the samples to 100 °C.

The presence of magnetite is demonstrated by a low coercivity (LC) component in the backfield curves (Fig. 4. e and i), the drop in susceptibility in the K/T curves around its Curie temperature of 580 °C, the reversibility (Fig. 4b, m) or quasi reversibility (Fig. 4f, g) of the K/T curves recorded in air (down to −196 °C) and the 'splitting' of the RT SIRM warming and cooling curves (e.g. Fig. 4c, l and n) around the Verwey transition (~110–120 K). The overall weak expression of the Verwey transition in our low T experiments may be explained by the presence of superparamagnetic magnetite grains (Moskowitz et al., 1989). The high coercivity mineral that prevents full AF demagnetization (after initial heating at 150 °C) of the NRM is likely hematite, in agreement with the pink color of the sediments. This is further supported by the decrease in the distance between the low temperature NRM demagnetization and NRM rewarming curves (after an initial thermal demagnetization of sample AK06 at 150 °C) below the Morin transition (250 K) in Fig. 4l. Sample AK06 also shows the presence of pyrrhotite by the drop in remanence below ~60 K in the low temperature demagnetization experiments. The presence of pyrrhotite in this sample is however blurred by the other magnetic minerals in the K/T curve (Fig. 4g).

Some of the remanence in most samples is however carried by a magnetic mineral that does not display any transition in the temperature-range of the MPMS measurements. The relative variation in magnetization in the low temperature experiments (i.e. the MPMS data) is very small. Therefore, some of the remanence is probably carried by maghemite (which displays the same behavior as magnetite in the backfield curves), that possibly formed as an oxidation rim around the magnetite particles.

5. Discussion

5.1. Calculated paleolatitudes

5.1.1. Paleozoic sites — SAB sediments

In the Paleozoic we predict the SAB to be part of Gondwana and located at its northern margin. Considering the possible ambiguity of the magnetic polarity of our data (due to the large rotations observed in most Cretaceous sites, see below), we calculated paleolatitudes assuming that the sampled sedimentary rocks could have been deposited either at southern or northern latitudes (Fig. 9a). For both possibilities, the paleolatitudes in the Permian and Triassic derived from sites AG, AM and AF + AI are unrealistically high for the Paleozoic, with AF + AI plotting close to the pole. On the northern, as well as on the southern hemisphere, the sites would fall within the Laurussian or Gondwana continent, respectively. The rocks from sites AM and AG were deposited during the Permo-Carboniferous Reverse Superchron (PCRS) and should therefore yield reverse polarities unless we coincidentally sampled one of the few subchrons — which is very unrealistic. For example, if the rocks at site AM have recorded a reverse polarity, they would have been deposited on the northern hemisphere and would have undergone a large counterclockwise rotation. For site AG, on the contrary, a reverse polarity remanence would imply a southern hemisphere origin and a large counterclockwise rotation. Clearly this is an impossible option for two nearby sites of similar age. Therefore, we infer that sites AG, AM and AF + AI have been remagnetized. Because site AM yields a positive fold test (Fig. 6), this suggests that the secondary magnetizations must have a pre-tilting origin. The single reverse polarity direction in site AL – although approximately antipodal to the normal polarity directions – does not provide any further constraints. For the remaining three sites in Paleozoic rocks (Famennian AL, Tournaisian AH and AE), a position in the northern hemisphere is unlikely (Fig. 9a). Assuming a southern hemisphere origin, the paleolatitudes from sites AL and AH plot at the northern margin

Fig. 6. Non-parametric fold tests (Tauxe and Watson, 1994) on locality P-combined, site AD and site AK. a–i) Fold tests carried out on all individual ChRM directions within a locality/site. j–r) Fold tests carried out on the mean ChRM direction calculated for all specimens with the same bedding plane orientation. a, d, g, j, m, p) Equal area plots of the ChRM before correction for bedding tilt (geographic coordinates) and b, e, h, k, n, q) after correction for bedding tilt (100% tilt correction). c, f, i, l, o, r) Results of the fold test based on 500 bootstrapped examples of the first eigenvalues (τ_1) upon progressive unfolding. The 95% bootstrap error is given above the diagrams.

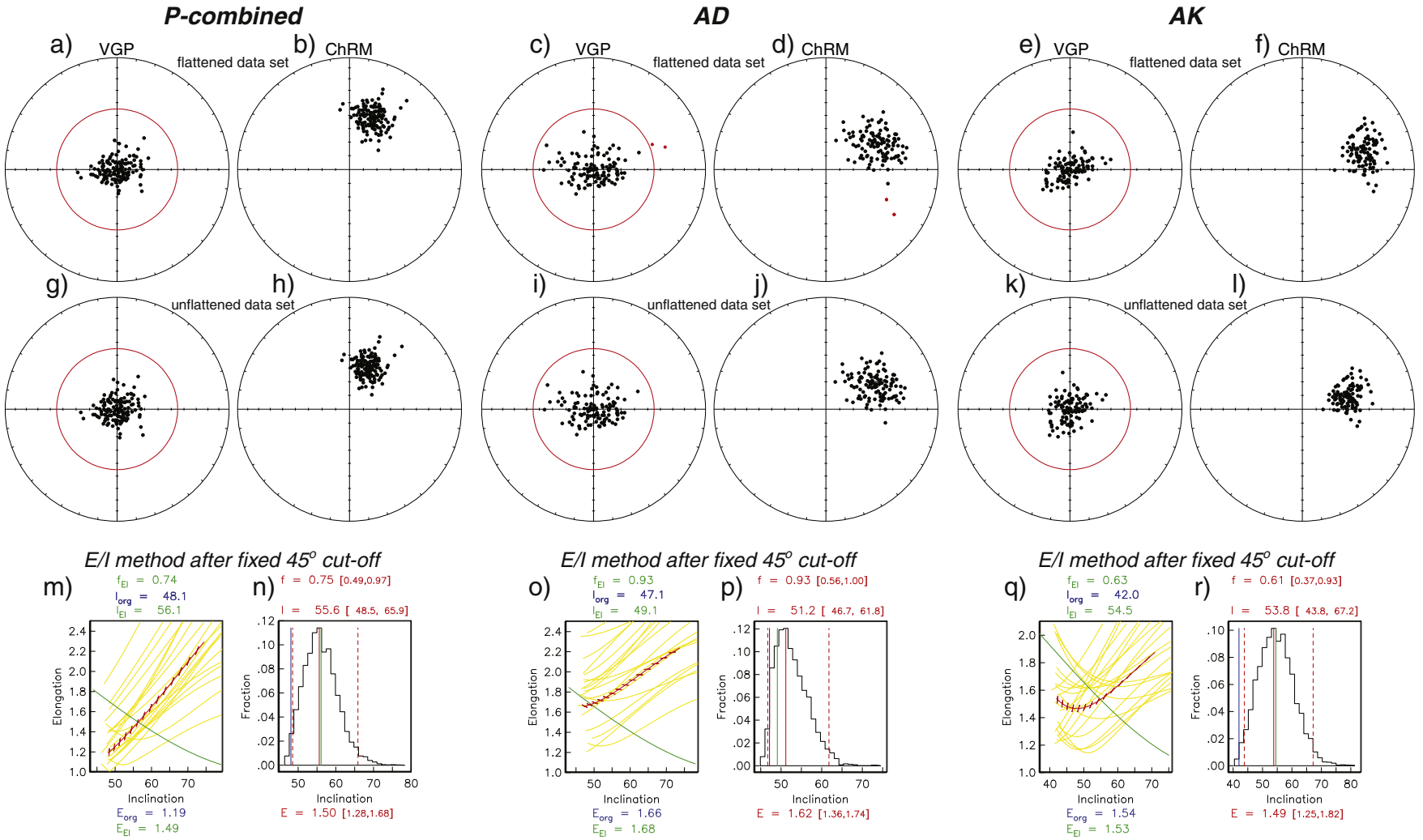

Fig. 7. Equal-area projections of the individual VGP directions before (a, c, e) and after (g, i, k) E/I correction. Equal-area projections of the individual ChRM directions before (b, d, f) and after (h, j, l) E/I correction (symbols as in Fig. 5) (Tauxe et al., 2008) after applying a 45° cut-off on the geomagnetic poles (red circle) with corresponding elongation vs. inclination (m, o, q) and fraction (of 5000 bootstraps) vs. inclination plots (n, p, r) for locality P and sites AD and AK. In the elongation vs. inclination plots the E/I for the TK03.GAD model (green line) and for the datasets (red barbed line) are plotted for different degrees of flattening. The red barbs indicate the direction of elongation: horizontal is E–W and vertical is N–S. Also shown are examples (yellow lines) from 20 (out of 5000) bootstrapped data sets. The crossing point (if the dataset intersects the model) represents the inclination/elongation pair most consistent with the TK03.GAD model, given as I_{EI} (in green) above the panel. I_{org} = original inclination, E_{org} = original elongation of the dataset, E_{EI} and I_{EI} are the elongation and inclination according to the E/I model, respectively. In the fraction/inclination plot, a histogram of intersecting points from 5000 bootstrapped data sets is shown. The most frequent inclination (solid red vertical line; dashed red vertical lines denote the 95% bootstrap error) is given with the error values on top of the panel. The inclinations of the original mean distribution (blue vertical line) and the inclination corresponding to the intersection of the data set with the model (green vertical line) are also indicated as well. E = the elongation (and error range) resulting from the bootstrapped data sets.

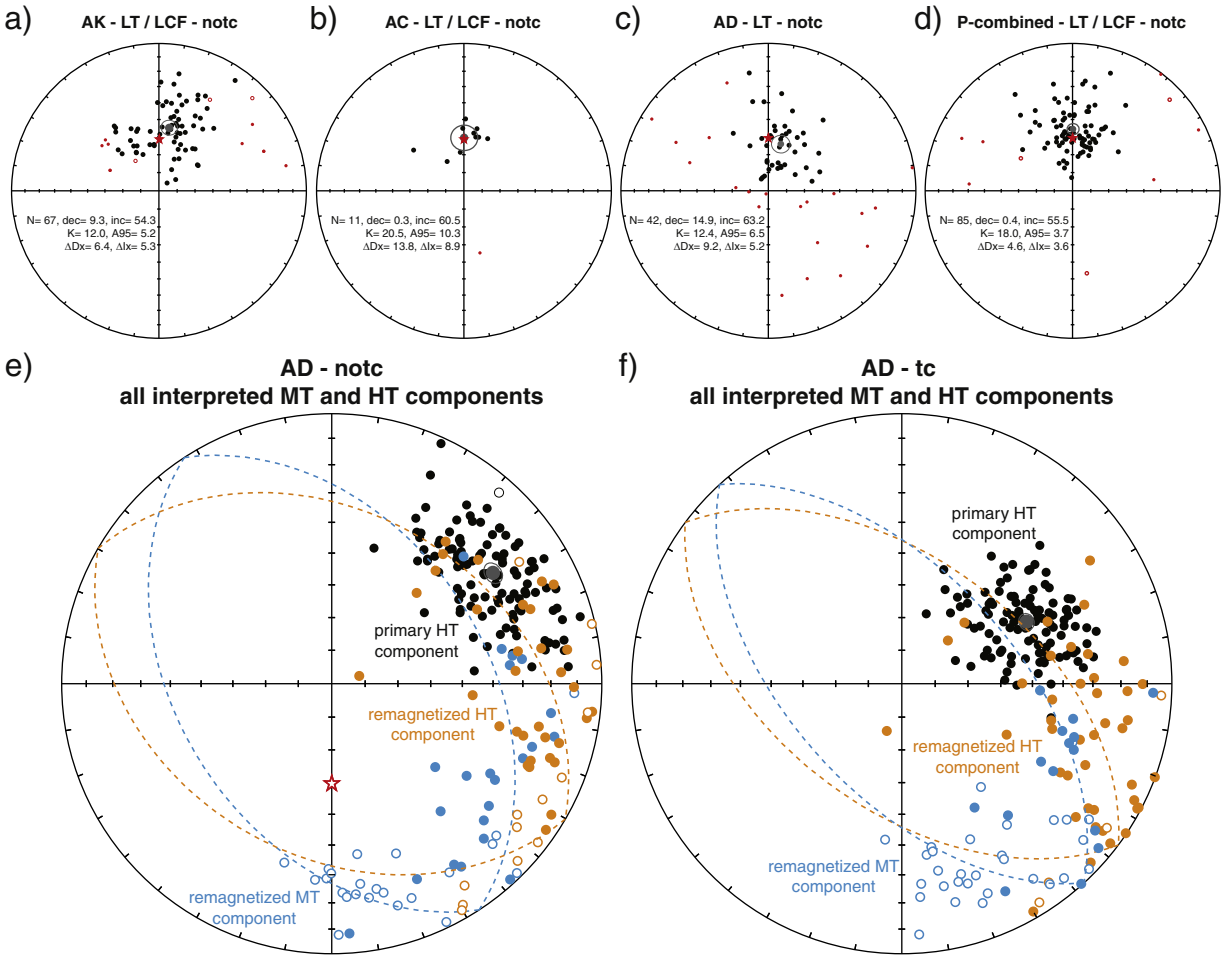

Fig. 8. Secondary magnetization components: a–d) Equal area projections of the low temperature (LT) and/or low coercive force (LCF) component of sites AK, AC and AD and locality P-combined before tilt correction. Open (closed) symbols denote projection on upper (lower) hemisphere. Large closed gray symbols surrounded by gray circles indicate respectively the mean LT/LCF components and their cone of confidence (α_{95}) before tilt correction (notc). Red open and closed (small) symbols indicate the individual directions rejected after applying a 45° cut-off on the virtual geomagnetic poles. Red stars indicate the present-day geocentric axial dipole (GAD) field direction at the sampling location. LT/LCF components for all four sites/localities are statistically indistinguishable or very close to this direction. Site/locality statistics are shown in the plot. Abbreviations as in Table 1. e–f) Equal area projections of (i) the primary high temperature (HT) ChRM directions of the first group of demagnetization diagrams (in black), (ii) the remagnetized medium temperature (MT; ~200–400 °C) component of the second group of samples (in blue) and (iii) the remagnetized high temperature (HT ~400–570 °C) component of the second group of samples (in orange) before (notc) and after (tc) tilt correction. Open (closed) symbols denote projection on upper (lower) hemisphere. Large closed gray symbol surrounded by a gray circle indicates respectively the mean ChRM direction of the primary HT component and its 95% cone of confidence (α95). Open red star indicates the reverse pre-Brunhes GAD field direction at the sampling locations. The dotted blue and orange great circles are the best fitted great circles through respectively all the individual MT and HT remagnetized components. Without correction for bedding tilt, none of these great circles include the reverse GAD field direction. Therefore, the secondary magnetization is probably not a relatively recent (>800 ka) post-tilting overprint.

of Gondwana, while site AE falls within the Paleo-Tethys ocean which separated Laurussia from Gondwana (c.f. Torsvik et al., 2012). Therefore, we cannot exclude the possibility that sites AL and AH carry a primary magnetization component of reverse polarity, acquired respectively during Famennian and Tournaisian times. However, we must take into account that the pre-Lower Carboniferous and Devonian APW paths are poorly determined because of the low number of available data sets of sufficient quality. Because the three sites sampled in the youngest Paleozoic rocks have been remagnetized, we surmise that the paleomagnetic signal from the oldest three Paleozoic sites is also secondary. Therefore, none of the six Paleozoic sites will be considered any further. Remagnetization may be related to Coniacian–Santonian ophiolite obduction and in the case of site AE to the intrusion of the sills.

5.1.2. Cretaceous sites — SAB and Eurasian margin sediments

The results from the Cretaceous Eurasian margin sedimentary rocks show that the rocks from site P5 are likely remagnetized. Data from site P7 will not be considered because of unreliable age constraints. The paleolatitudes of the Cretaceous sites/locality (AC, AD, AK and P-combined) that we infer to carry a primary ChRM magnetization and the paleolatitudes corrected for inclination shallowing (AD, AK and P-combined) are given in Fig. 9a and c and Table 1. The paleolatitudes for each Cretaceous site are plotted on the Eurasian paleolatitude versus age curve, derived from the most recent Global Apparent Polar Wander Path (GAPWaP) of Torsvik et al. (2012). In this GAPWaP, all data from detrital sedimentary rocks that were not corrected for inclination shallowing in the original studies were corrected for inclination shallowing assuming an average flattening factor of 0.6, following King (1955):

$$\tan I_{obs} = f \quad \tan \quad I_f. \tag{1}$$

The value of f = 0.6 is a 'best guess' however, because values provided in a compilation by Bilardello and Kodama (2010) range from 0.40 to 0.83 for hematite bearing rocks and from 0.54 to 0.79 for magnetite

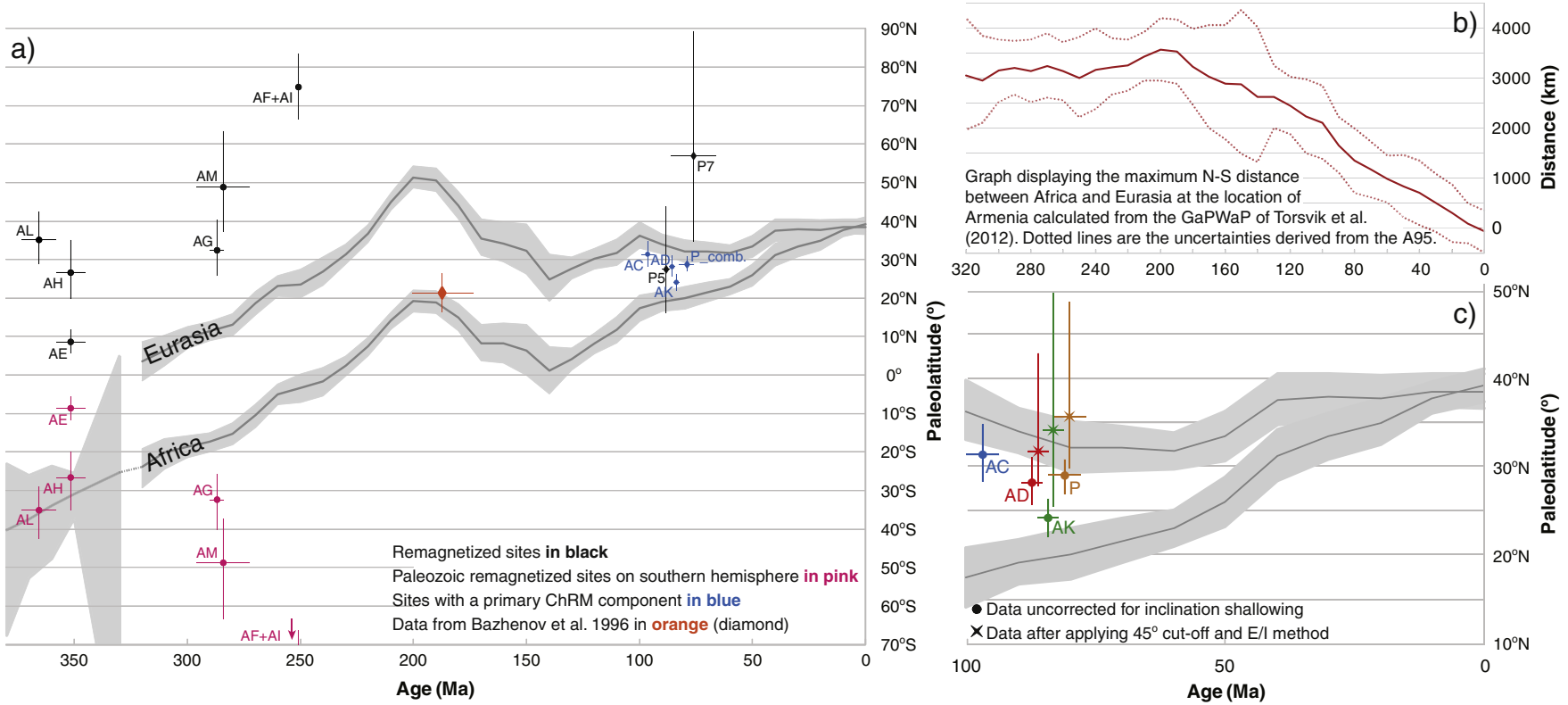

Fig. 9. a) and c) Paleolatitude versus age plots: The two curves and their shaded envelopes (Δλ, the 95% confidence level on the paleolatitude) are calculated from the African and Eurasian Global Apparent Polar Wander Path (GAPWaP) of Torsvik et al. (2012), for the time period 320–0 Ma, for a reference mean site in the SAB situated at 39.3°N and 45.4°E, assuming that the SAB was lying in its present position relative to respectively Africa and Eurasia. In a) the lower curve is calculated from the Gondwana APW path between 380 and 330 Ma. The curve at 340 Ma is an interpolation of the curve between 330 and 350 Ma, as a result of the absence of reliable data at 340 Ma. We chose to interpolate the Δλ error envelope between 330 and 350 Ma as well. All used APW paths assume a flattening factor of 0.6 for detrital sediments (Torsvik et al., 2012) that were not corrected for inclination shallowing in the original studies. A 95% confidence level (Δλ error envelope) was calculated from ΔI_x. a) For the Paleozoic rocks, the remagnetized data from this study are plotted in black, assuming that the rocks were deposited in the northern hemisphere as well as in pink, assuming a they were deposited in the southern hemisphere. The data from the non-remagnetized Cretaceous rocks are plotted in blue. b) Distance (km) versus age (Ma) plot showing the decreasing width of the Tethys ocean with time at the position of Armenia. The width of the oceanic basin remains approximately constant at ~3000–3500 km until 190 Ma after which the domain closes at a fairly constant rate. c) Enlarged a). Data from site AD (in red), AK (in green) and locality P-combined (in brown) are plotted before as well as after the E/I correction for inclination shallowing.

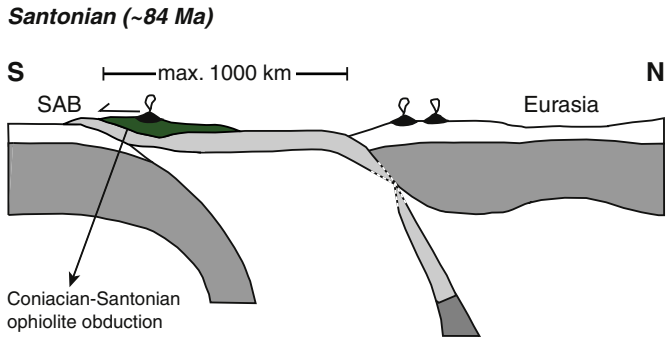

Fig. 10. Schematic N–S cross-section of the study area in the Santonian (~84 Ma). In the Coniacian–Santonian the SAB was obducted by ophiolites. The pink pelagic limestones sampled at sites AD and AK were deposited on top of these obducted ophiolites. The maximum allowable N–S distance (1000 km) between the SAB and the Eurasian margin is indicated. This distance is likely shorter however.

bearing rocks. The introduction of a fixed flattening factor of 0.6 to the GAPWaP introduces some uncertainty, but is at present the most realistic approximation.

As mentioned earlier, reliable paleolatitude reconstructions since the Cretaceous in this part of the Tethyan realm are challenging, because of the relatively narrow remnant oceanic basin and the uncertainties in the pole paths and data. In Fig. 9b the width of the oceanic Tethyan domain between Africa and Eurasia at the position of Armenia derived from the GAPWaP (Torsvik et al., 2012) is displayed as a function of time. For the Cretaceous to Present, errors derived from the A95 of the GAPWaP are typically on the order of ±500–600 km, which translates to a maximum total uncertainty of 1200 km. Between 170 and 140 Ma the error margins are even larger, because of the absence of reliable Middle–Upper Jurassic poles; the maximum uncertainty may even reach up to several thousands of kilometers between 140 and 150 Ma (i.e. around the Jurassic–Cretaceous boundary). Furthermore, the paleolatitude error of paleomagnetic data sets is optimally in the order of ±2°–3°, but the error resulting from the bootstrap of the E/I method is larger (see Table 1, Figs. 7 and 9). In our study area, the north–south width of the Tethys ocean is fairly constant between 320 Ma and 190 Ma (Fig. 9b). In the Early Jurassic the north–south width of the oceanic basin between Africa and Eurasia begins to decrease with a relatively uniform rate from (roughly) 3500 ± 500 km at 200 Ma to 1500 ± 500 km at 80 Ma. Paleomagnetic data from our study region that are used for paleolatitude reconstructions should therefore be interpreted with these considerations in mind. The interpretation of geologic observations has led to different views on the timing of SAB–Eurasia collision. Sosson et al. (2010) argue for collision of the SAB with Eurasia in the Paleocene to Middle Eocene and support the existence of a remnant oceanic basin between the SAB and the Eurasian margin in the Late Cretaceous by 1) ongoing arc magmatic activity

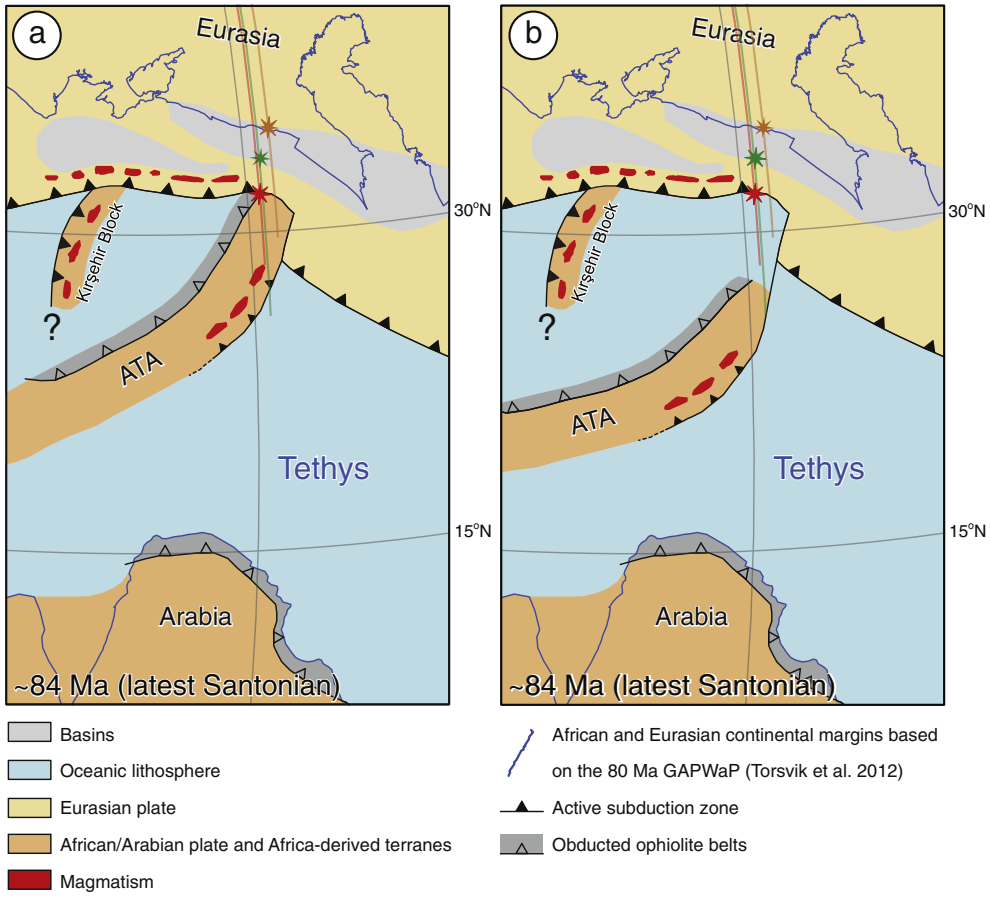

Fig. 11. Paleogeographic reconstructions at ~84 Ma (latest Santonian) after Barrier and Vrielynck (2008) and Hässig et al. (2013). The positions of the Eurasian and African/Arabian continental margins are based on the 80 Ma GAPWaP of Torsvik et al. (2012). The width of ATA is an approximation because there are no restored cross sections available for the Anatolides, Taurides and SAB. Red (green) stars indicate the paleolatitude positions of sites AD (AK) with their error bars (resulting from the E/I method) that were sampled within the SAB. Same for the brown star for locality P-combined sampled in Eurasian margin sediments. a) and b): ATA in its plausible respective northern and southern paleolatitude position (see text for explanation). The uncertainty of the position of the African/Arabian and Eurasian continents derived from the GAPWaP is not displayed in this figure. This leads to a smaller N–S distance in b) than the calculated maximum of ~1000 km.

that ceases before the Maastrichtian on the Eurasian margin (Adamia et al., 2011), resulting from the subduction of oceanic lithosphere below Eurasia and 2) the occurrence of remnant oceanic crust covered by pelagic Campanian–Maastrichtian limestones to the north of the obduction front. They would further argue that a southwest vergent tectonic event affects the ophiolites, volcanic arc and the Paleocene foreland basin before the deposition of late-Middle to Late Eocene as a result of collision. Rolland et al. (2012), however, propose closure of the oceanic basin between the SAB and Eurasia in the Late Cretaceous, at ~80–75 Ma, only several millions of years after ophiolite obduction. This Campanian age is based on 1) the onset of subduction south of the ATA microplate around 95 Ma, 2) the presence of crystalline blocks likely derived from the Eurasian margin in the Coniacian–Santonian flysch below the Campanian–Maastrichtian limestones and 3) the final stage of epidote–amphibolite-grade deformation in the Stepanavan blueschists at 74–71 Ma, suggesting the amalgamation of the SAB with the Eurasian margin at that time (Rolland et al., 2009a). The occurrence of arc-related volcanic rocks of Maastrichtian to Paleocene age in the eastern Pontides and the Lesser Caucasus, as well as tectonostratigraphic data (Adamia et al., 2011; Altherr et al., 2008; Okay and Şahintürk, 1997; Robertson et al., 2014; Robinson et al., 1995; Sosson et al., 2010) that support a Paleocene to Eocene collision age are however in conflict with a Campanian collision age. However, we must keep in mind here that actual collision ages may vary along the former Eurasian margin. Variations could result from pre-defined geometries of the continental margins (i.e. Eurasia and the ATA microplate) and the effect of oblique subduction. The collision of the Kırşehir Block (Fig. 1) with the Eurasian margin in the central Pontides in the latest Cretaceous or Paleocene (Lefebvre et al., 2013; Meijers et al., 2010c) possibly obscures the record of ATA–Eurasia collision in the central Pontides.

When comparing our data to the Eurasian curve, we take both the error at the 95% confidence level on the Eurasian curve (shaded area on Fig. 9a and c) and the 95% bootstrap error resulting from the E/I method (sites P, AD, AK) or ΔI_x (site AC) into account. After correction for inclination shallowing, locality P-combined, which was sampled in Eurasian margin sedimentary rocks, falls within error on the Eurasian curve. This is also the case for the Cretaceous sites from the SAB: the corrected paleolatitudes of the two Santonian (~85 Ma) sites AD and AK and the uncorrected paleolatitude of the Cenomanian (~97 Ma) site AC are south of locality P-combined, but not statistically different from the paleolatitude of the Eurasian curve. Therefore, we cannot distinguish our data from the Eurasian paleolatitude versus age curve. This suggests that the SAB could have been already accreted to Eurasia by the Cenomanian/Santonian. However, if we take into account the errors associated with the paleolatitude versus age curves of Fig. 9c and the errors associated with our data, the maximum possible distance between SAB and Eurasia for each one of our Cretaceous sites can be calculated. This maximum distance is given by the difference between the upper limit of the shaded envelop on the Eurasian curve and the lower limit of the error bar associated with each site. For site AC (~97 Ma) this is ~1200 km. For sites AK and AD (~85 Ma) this is respectively ~1100 and 900 km, so on average ~1000 km, after correction for inclination shallowing with the E/I method and taking the bootstrap error into account. This maximum ~1000 km N–S distance is illustrated in a cross-section in Fig. 10.

Alternatively we can estimate the maximum possible distance between SAB and Eurasia by comparing the paleolatitudes calculated from locality P-combined (originally belonging to the Eurasian margin) and sites AD and AK (of Gondwana origin) after E/I correction. The paleolatitudes of sites AD and AK (SAB) are very similar (31.9°N and 34.3°N respectively) and an approximate average of these values would be ~33.1°N for these Santonian sites. Compared to the paleolatitude of locality P-combined (36.1°N; which is ~4.5 Ma younger) the difference is ~3°. This corresponds to a N–S width of ~350 km (uncorrected for shortening within the orogenic belt), which would suggest a very limited remnant basin between the SAB and Eurasia after ophiolite obduction. Although our results are in slightly better agreement with an ocean closure in the Late Cretaceous, our data do not really allow us to determine the age of continental collision.

A limited number of available studies from the Pontides could potentially constrain the paleolatitude of the southern Eurasian margin in the Santonian–Coniacian (e.g. Channell et al., 1996; Hisarlı, 2011; van der Voo, 1968). Practically all published studies were however (partially) carried out on sedimentary rocks and those data sets were not corrected for inclination shallowing. Only two data sets from the central Pontides were corrected for inclination shallowing (Meijers et al., 2010c). The corrected data suggest that the southern margin of Eurasia in the central Pontides was located at lower latitudes in the Coniacian–Santonian ($\lambda = 26.6°$ and $\lambda = 31.3°$, respectively) than in present-day Armenia in the Lower Campanian (locality P-combined, $\lambda = 36.1°$). Statistically, the paleolatitudes are however indistinguishable (95% bootstrap error) from each other and from the Eurasian paleolatitude curve and we therefore did not incorporate these data directly into the paleogeographic reconstructions discussed below, although they would leave some space for a more southerly margin of Eurasia westward of present-day Armenia and Georgia (provided that the time gap between the deposition of the Coniacian-Santonian rocks (sampled in Turkey) and the Lower Campanian rocks (sampled in Armenia) is negligible).

Two paleogeographic reconstructions (Fig. 11) illustrate the possible position of the SAB with respect to the African/Arabian and Eurasian margins at ~84 Ma (latest Santonian). The westward continuation of the SAB into the Anatolides and Taurides (i.e. the ATA microplate), as well as the position of obducted ophiolites, subduction zones and volcanic arcs is based on the paleogeographic reconstructions by Barrier and Vrielynck (2008), Sosson et al. (2010) and Hässig et al. (2013). The paleogeography in the Late Cretaceous is illustrated in two subfigures (Fig. 11). In Fig. 11a, the northern location of the ATA in the latest Santonian is shown, i.e. at the southern margin of Eurasia, considering the calculated paleolatitudes of sites AD and AK (Table 1). Fig. 11b shows the southern location of the ATA in the Santonian based on the maximum possible distance between the SAB and Eurasia derived from sites AD and AK. The orientation of the ATA microplate is poorly determined. The only paleomagnetic data from Bazhenov et al. (1996) suggest a ~20° clockwise rotation of the SAB since the Early Jurassic, hence the ENE–WSW 'strike' of ATA in the Tethys ocean (Fig. 11a and b) compared to its present more E–W 'strike', leading to a westward widening oceanic basin between ATA and Eurasia. Data from the western extent of ATA (western and west-central Taurides) show variable results (Meijers et al., 2011 and references therein), and the orientation of ATA is poorly defined. The uncertainty of the orientation of ATA within the Tethyan realm as well as its exact paleolatitude leads us to present the two different options in Fig. 11. The geometric reconstruction of the plutons of the Central Anatolian Crystalline Complex that are part of the Kırşehir Block (Lefebvre et al., 2013) requires an oceanic basin between ATA and the Eurasian margin that widens westward, when adopting a Late Cretaceous collision age of the SAB with Eurasia. This could be interpreted as support for an ENE–WSW oriented ATA. Geologic data show however stronger evidence for a Paleocene collision age. Lefebvre (2011) presents evidence for an eastward dipping subduction zone below the Kırşehir Block in the Late Cretaceous, based on a study of its metamorphic and magmatic rocks, as well as a paleomagnetic reconstruction of the magmatic belts (Lefebvre et al., 2013). This complicates the paleogeography of the Tethyan realm in the Late Cretaceous, because the southward continuation of this subduction zone and its possible link to other subduction zones is unclear and needs to be

constrained by new data, hence the question mark in both proposed paleogeographic reconstructions.

5.2. Vertical axis rotations

Bazhenov and Burtman (2002) defined the eastern Pontides–Lesser Caucasus (Fig. 1) as a northward convex orocline based on a paleomagnetic study on Cretaceous to Eocene sedimentary rocks. Their hypothesis was confirmed by new data from the eastern Pontides by Hisarlı (2011). The Cretaceous and Eocene rocks from both limbs of the orocline have been rotated (see arrows in Fig. 1), implying that orocline formation took place after the Eocene. Orocline formation in the eastern Pontides–Lesser Caucasus fold and thrust belt therefore postdates latest Cretaceous or Paleocene orocline formation related to collision of the Kırşehir Block of African affinity with the Eurasian margin in the central Pontides (Meijers et al., 2010c). To date the age of the eastern Pontides–Lesser Caucasus orocline, a study of rocks deposited after the Eocene is necessary and at present we can only compare our results to the findings of Bazhenov and Burtman (2002). Their study includes data from Bazhenov and Burtman (1989) and Bolshakov and Solodovnikov (1981) that were obtained in the eastern, clockwise (CW) rotated limb of the orocline in Armenia. Assuming that the rotation pole is close to the site, a vertical axis rotation experienced by this site can be estimated. In the eastern limb of the orocline in Armenia, the expected Cretaceous declination for Eurasia is ~10°. Compared with the expected direction, the synthesis of Bazhenov and Burtman (2002) shows CW rotations ranging from ~4 to 46° in Upper Cretaceous rocks from this part of the orocline. Note that in the western part of the Lesser Caucasus, Bazhenov and Burtman (2002) observed mixed rotations (i.e. clockwise, counterclockwise and zero rotations) in rocks of Middle Eocene age. Our four sites in Upper Cretaceous sedimentary rocks show CW rotations. For locality P on the Eurasian margin the rotation is 11.5° CW, in agreement with the data presented in Bazhenov and Burtman (2002). The three sites sampled on the SAB (AC, AD and AK) show larger CW rotations of 42°, 54° and 65° respectively. This possibly implies that the sedimentary rocks deposited on the SAB were also affected by oroclinal bending in the eastern Pontides–Lesser Caucasus fold-and-thrust belt. To better understand the cause of oroclinal bending in this region, data bearing on the history and evolution of post-Eocene rotations in this region are needed.

6. Conclusions

We show that six sites in Paleozoic rocks analyzed in this study have been (AG, AM, AF + AI) or likely have been (AL, AH, AE) remagnetized, possibly as a result of ophiolite obduction in the Coniacian–Santonian. Therefore these results are not suitable for paleogeographic reconstructions. Four sites/localities in Upper Cretaceous strata however, carry a primary remanence, supported by positive fold tests in site AD and locality P. The extensive sampling (>100 samples) of two Santonian sites from the SAB (sites AD and AK) and from the Lower Campanian locality P from the Eurasian margin allow us to statistically correct for inclination shallowing commonly recorded in sediments and the associated underestimated paleolatitudes, using the E/I method of Tauxe and Kent (2004). The corrected paleolatitudes for these three sites/localities fall on the paleolatitude curve for Eurasia, deduced from the GAPWaP (Torsvik et al., 2012). This would suggest that the oceanic domain between the SAB and Eurasia was already closed by the Santonian, which is in disagreement with most geologic data that time the collision. However, if we take the error bars associated with the SAB sites (AD and AK), as well as the errors on the reference paleolatitude curves for Eurasia into account, a maximum possible width of ~1000 km between SAB and Eurasia in the Santonian is possible.

We provide a tentative estimate on this width by comparing the N–S distance between locality P-combined (belonging to the Eurasian margin) and sites AD and AK (belonging to the SAB), which leads to a maximum N–S width of ~350 km (uncorrected for shortening within the orogenic belt). The resolution of the pole path and our paleomagnetic data do therefore not allow us to distinguish between a model that suggests near-simultaneous closure of the oceanic basin between the SAB and the Eurasian margin, and ophiolite obduction onto the SAB by the Late Cretaceous (Rolland et al., 2012) and geologic data that support the presence of a narrow remnant oceanic basin between the SAB and the Eurasian margin until the Paleocene (Adamia et al., 2011; Altherr et al., 2008; Okay and Şahintürk, 1997; Robertson et al., 2014; Robinson et al., 1995; Sosson et al., 2010).

The clockwise vertical axis rotations documented by the paleomagnetic data from Upper Cretaceous strata of this study are in line with the results presented by Bazhenov and Burtman (2002) that lead to the hypothesis that the arcuate shape of the Lesser Caucasus is caused by oroclinal bending.

Acknowledgments

The field work and analyses were supported by the Darius Programme. The authors would specifically like to thank the coordination and support of E. Barrier and M.F. Brunet. MJMM would like to thank the Henri Poincaré Postdoctoral Fellowship under which this research was carried out at the Observatoire de la Côte d'Azur (Nice). The authors would like to thank the following persons for their assistance in the field: Gayané Asatryan, Musegh Mkrtchyan, Sargis Vardanyan and drivers Hayro, Marat and Stephan. We also thank the staff at the Institute for Rock Magnetism at the University of Minnesota and especially Mike Jackson and Dario Bilardello for their help in carrying out and interpreting part of the rock magnetic measurements and Douwe van Hinsbergen for providing the paleogeographic reconstruction of the major continents. UK would like to acknowledge Ivan Gabrielyan and Tigran Lorsabyan for their help during a first reconnaissance field work. The authors would like to thank the Editor (Laurent Jolivet), John Geissman and Aral Okay for their helpful comments and constructive reviews, as well as three reviewers of an earlier version of this manuscript: Jérôme Gattacceca, Rob van der Voo and an anonymous reviewer.

Appendix A. Supplementary material

Supplementary data to this article can be found online at http://dx.doi.org/10.1016/j.tecto.2015.01.012.

References

Abramyan, M.S., 1951. The stratigraphy and fauna of Brachiopoda in the Late Famennian and Etroeungt (Paleozoic) deposits in the Armenian SSR. Archive of the IGS of the Academy of Sciences of the Armenian SSR (in Russian).

Adamia, S.A. (Ed.), 1984. Prealpine basement of the Caucasus — composition, structure, and formation. Tectonika I Metallogenia Kavkaza 86. Metsniereba, Tbilisi (3–104 pp.).

Adamia, S., Bergougnan, H., Fourquin, C., Haghipour, A., Lordkipanidze, M., Özgül, N., Ricou, L., Zakariadze, G., 1980. The Alpine Middle East between the Aegean and the Oman traverses. 26th International Geological Congress Paris C5pp. 122–136.

Adamia, S.A., Kekelia, M., Tsimakuridze, 1983. Pre-Variscan and Variscan granitoids of the Caucasus. IGCP Newsl. 5, 5–10.

Adamia, S., Zakariadze, G., Chkhotua, T., Sadradze, N., Tsereteli, N., Chabukiani, A., Gventsadze, A., 2011. Geology of the Caucasus: a review. Turk. J. Earth Sci. 20, 489–544. http://dx.doi.org/10.3906/yer-1005-11.

Aghamalyan, V.A., 1978. The old metamorphic complexes of the territory of Armenian SSR and their tectonic disposition. Proceedings of Reports of the Second Regional Petrographic Symposium on Caucasus, Crimea and Carpathians, Tbilisi, pp. 109–115 (in Russian).

Aghamalyan, V.A., 1998. The Basement Crystalline of Armenia, Yerevan (in Russian).

Altherr, R., Topuz, G., Siebel, W., Şen, C., Meyer, H.-P., Satır, M., Lahaye, Y., 2008. Geochemical and Sr–Nd–Pb isotopic characteristics of Paleocene plagioleucitites from the Eastern Pontides (NE Turkey). Lithos 105, 149–161. http://dx.doi.org/10.1016/j.lithos.2008.03.001.

Anson, G.L., Kodama, K.P., 1987. Compaction-induced inclination shallowing of the post-depositional remanent magnetization in a synthetic sediment. Geophys. J. R. Astron. Soc. 88, 673–692.

Arakelyan, R.A., 1950. The stratigraphy of Paleozoic deposits in southwestern Armenia and adjacent areas of Nakhijevan ASSR. Archive of the IGS of the Academy of Sciences of the Armenian SSR.

Arakelyan, R.A., 1964. The Paleozoic–Mesozoic. The Geology of the Armenian SSR: Stratigraphy. Publishing House of the Academy of Sciences of the Armenian SSR, pp. 21–63 (in Russian).

Asatryan, G., Danelian, T., Seyler, M., Sahakyan, L., Galoyan, G., Sosson, M., Avagyan, A., Hubert, B., Person, A., Vantalon, S., 2012. Latest Jurassic–Early Cretaceous Radiolarian assemblages constrain episodes of submarine volcanic activity in the Tethyan oceanic realm of the Sevan ophiolites (Armenia). In: Danelian, T., Goričan, S. (Eds.), Radiolarian Biochronology as a Key to Tectono-stratigraphic Reconstructions. Bulletin de la Société Géologique de France 183, pp. 319–330.

Barrier, E., Vrielynck, B., 2008. Palaeotectonic map of the Middle East, Atlas of 14 maps, Tectonosedimentary–Palinspastic maps from Late Norian to Pliocene. Commission for the Geologic Map of the World (CCMW, CCGM), Paris, France.

Bazhenov, M., Burtman, V.S., 1989. Paleomagnetism of Upper Cretaceous rocks from the Caucasus and its implications for tectonics. In: Sengor, A.M.C. (Ed.), Tectonic Evolution of the Tethyan Region. Kluwer Academic Publishing, Dordrecht, pp. 217–239.

Bazhenov, M.L., Burtman, V.S., 2002. Eocene paleomagnetism of the Caucasus (southwest Georgia): oroclinal bending in the Arabian syntaxis. Tectonophysics 344 (3–4), 247–259.

Bazhenov, M., Burtman, V.S., Levashova, N., 1996. Lower and Middle Jurassic paleomagnetic results from the south Lesser Caucasus and the evolution of the Mesozoic Tethys Ocean. Earth Planet. Sci. Lett. 141, 79–89.

Belov, A.A., Sokolov, S.D., 1973. Relics of Mesozoic oceanic crust among the crystalline complexes of the Miskhana massif of Armenia. Soviet Geol. 8, 26–41 (in Russian).

Belov, A.A., Bragin, N.Yu., Vishnevskaya, V.S., Satian, M., Sokolov, S.D., 1991. New data about the age of the ophiolites of Vedi (Armenia). Reports of the USSR Academy of Science 321 pp. 784–787 (in Russian).

Besse, J., Courtillot, V., 2002. Apparent and true polar wander and the geometry of the geomagnetic field in the last 200 million years. J. Geophys. Res. 107 (B11). http://dx.doi.org/10.1029/2000JB000050.

Bilardello, D., 2013. Understanding DRM acquisition of plates and spheres: a first comparative experimental approach. Geophys. J. Int. 195 (1), 148–158. http://dx.doi.org/10.1093/gji/ggt240.

Bilardello, D., Kodama, K.P., 2010. Rock magnetic evidence for inclination shallowing in the early Carboniferous Deer Lake Group red beds of western Newfoundland. Geophys. J. Int. 181, 275–289. http://dx.doi.org/10.1111/j.1365-246X.2010.04537.x.

Bolshakov, A.S., Solodovnikov, G.M., 1981. Intensity of the geomagnetic field in the Late Cretaceous. Izv. Akad. Nauk SSSR, Ser. Fiz. Zemli 10, 58–68 (in Russian).

Butler, R.F., 1992. Paleomagnetism: Magnetic Domains to Geologic Terranes. Blackwell Scientific Publications, Boston (319 pp.).

Celaya, M.A., Clement, B.M., 1988. Inclination shallowing in deep sea sediments from the North Atlantic. Geophys. Res. Lett. 15. http://dx.doi.org/10.1029/GL015i001p00052.

Channell, J.E.T., Tüysüz, O., Bektaş, O., Şengör, A.M.C., 1996. Jurassic–Cretaceous paleomagnetism and paleogeography of the Pontides (Turkey). Tectonics 15, 201–212. http://dx.doi.org/10.1029/95TC02290.

Creer, K.M., Irving, E., Nairn, A.E.M., 1959. Paleomagnetism of the Great Whin Sill. Geophys. J. R. Astron. Soc. 2, 306–323.

Danelian, T., Asatryan, G., Sosson, M., Person, A., Sahakyan, L., Galoyan, G., 2008. Discovery of two distinct Middle Jurassic Radiolarian assemblages in the sedimentary cover of the Vedi ophiolite (Lesser Caucasus, Armenia). C. R. Palevol 7, 324–334.

Danelian, T., Asatryan, G., Sahakyan, L., Galoyan, Gh., Sosson, M., Avagyan, A., 2010. New and revised Radiolarian biochronology for the sedimentary cover of ophiolites in the Lesser Caucasus (Armenia). In: Sosson, M., Kaymakci, N., Stephenson, R.A., Bergerat, F., Starostenko, V. (Eds.), Sedimentary Basin Tectonics from the Black Sea and the Caucasus to the Arabian Platform 340. Geological Society Special Publications, London, pp. 383–391.

Danelian, T., Asatryan, G., Galoyan, G., Sosson, M., Sahakyan, L., Caridroit, M., Avagyan, A., 2012. Geological history of ophiolites in the Lesser Caucasus and correlation with the Izmir–Ankara–Erzincan suture zone: insights from radiolarian biochronology. In: Danelian, T., Goričan, S. (Eds.), Radiolarian Biochronology as a Key to Tectono-stratigraphic Reconstructions. Bulletin de la Société Géologique de France 183, pp. 331–342.

Danelian, T., Zambetakis-Lekkas, A., Galoyan, G., Sosson, M., Asatryan, G., Sahakyan, L., Hubbert, B., Grigoryan, A., 2014. Reconstructing Upper Cretaceous (Cenomanian) paleoenvironments in Armenia based on Radiolaria and benthic Foraminifera; implications for the geodynamic evolution of the Tethyan realm in the Lesser Caucasus. Palaeogeogr. Palaeoclimatol. Palaeoecol. 413, 123–132. http://dx.doi.org/10.1016/j.palaeo.2014.03.011.

Deenen, M.H.L., Ruhl, M., Bonis, N.R., Krijgsman, W., Kuerschner, W.M., Reitsma, M., van Bergen, M.J., 2010. A new chronology for the end-Triassic mass extinction. Earth Planet. Sci. Lett. 291, 113–125.

Deenen, M.H.L., Langereis, C.G., van Hinsbergen, D.J.J., Biggin, A.J., 2011. Geomagnetic secular variation and the statistics of palaeomagnetic directions. Geophys. J. Int. 186, 509–520.

Dietz, R.S., 1961. Continent and ocean basin evolution by spreading of the sea floor. Nature 190, 854–857.

Eghoyan, V.L., 1955. The Upper-Cretaceous Deposits of the South-Western Part of Armenian SSR. Izdatelstvo National Academy of Sciences Armenia SSR (in Russian).

Fisher, D.A., 1953. Dispersion on a sphere. Proc. R. Soc. London, Ser. A 217, 295–305.

Galoyan, G., 2008. Etudes Pétrologiques, Géochimiques et Géochronologiques des Ophiolites du Petit Caucase (Arménie). (PhD Thesis). University of Nice-Sophia Antipolis.

Galoyan, G., Rolland, Y., Sosson, M., Corsini, M., Melkonian, R., 2007. Evidence for superposed MORB, oceanic plateau and volcanis arc series in the Lesser Caucasus (Stepanavan, Armenia). C. R. Geosci. 339, 482–492.

Galoyan, G., Rolland, Y., Sosson, M., Corsini, M., Billo, S., Verati, C., Melkonyan, R., 2009. Geology, geochemistry and $^{40}Ar/^{39}Ar$ dating of Sevan ophiolites (Lesser Caucasus, Armenia): evidence for Jurassic Back-arc opening and hot spot event between the South Armenian Block and Eurasia. J. Asian Earth Sci. 34, 135–153.

Ginter, M., Hairapetian, V., Grigorian, A., 2011. Chondrichthyan microfossils from the Famennian and Tournaisian of Armenia. Acta Geol. Pol. 61 (2), 153–173.

Gong, Z., Langereis, C.G., Mullender, T.A.T., 2008. The rotation of Iberia during the Aptian and the opening of the Bay of Biscay. Earth Planet. Sci. Lett. 273 (1–2), 80–93.

Grigoryan, A., 1990. The conodonts of the Permian–Triassic limit in Armenia. (PhD thesis), University of Moscow (in Russian).

Grigoryan, A., Alekseev, A.S., Yoahimski, M., 2012. Discontinuation on the boundary between Middle and Upper Permian in Armenia (Abstract). Annual Meeting (conference) of the Section Paleontology. Moscow Society of Nature Investigators, Section of Paleontology. Paleontological Institute of Borisyak A. A., Russian Academy of Sciences, Moscow, pp. 25–26.

Hakobyan, V.T., 1978. Biostratigraphy of the Upper Cretaceous Deposits of Armenian SSR. Izdatelstvo National Academy of Sciences Armenia SSR (in Russian).

Hässig, M., Rolland, Y., Sosson, M., Galoyan, G., Müller, C., Avagyan, A., Sahakyan, L., 2013. Geology and structure of the Amasia ophiolites, NW Sevan–Akera suture zone, Lesser Caucasus, insights for a large-scale obduction in Armenia and NE Turkey. Tectonophysics 588, 135–153. http://dx.doi.org/10.1016/j.tecto.2012.12.003.

Hässig, M., Rolland, Y., Sahakyan, L., Sosson, M., Galoyan, G., Avagyan, A., Bosch, D., Müller, C., 2014. Multi-stage metamorphism in the South Armenian Block during the Late Jurassic to Early Cretaceous: tectonics over south-dipping subduction of Northern branch of Neotethys. J. Asian Earth Sci. http://dx.doi.org/10.1016/j.jseaes.2014.07.018.

Heezen, B.C., 1960. The rift in the ocean floor. Sci. Am. 203, 98–110.

Hisarlı, Z.M., 2011. New paleomagnetic constraints on the late Cretaceous and early Cenozoictectonic history of the Eastern Pontides. J. Geodyn. 52, 114–128. http://dx.doi.org/10.1016/j.jog.2010.12.004.

Hodych, J.P., Bijaksana, S., 1993. Can remanence anisotropy detect paleomagnetic inclination shallowing due to compaction? A case study using cretaceous deep-sea limestones. J. Geophys. Res. (ISSN: 0148-0227) 98. http://dx.doi.org/10.1029/93JA02022.

Jackson, M., Banerjee, S.K., Marvin, J.A., Lu, R., Gruber, W., 1991. Detrital remanence inclination errors and anhysteretic remanence anisotropy: quantitative model and experimental results. Geophys. J. Int. 104, 95–103.

Karyakin, Y.V., 1989. Geodynamics of the Formation of the Volcanic Complexes of the Lesser Caucasus, Moscow 'Nauka'.

Kharazian (Author Ed.) and Sargsyan (Ed.), 2005. Geological map of republic of Armenia. Yerevan: Ministry of Nature Protection of Republic of Armenia, Geological Agency, map: National government publication.

Kim, B., Kodama, K.P., 2004. A compaction correction for the paleomagnetism of the Nanaimo Group sedimentary rocks: Implications for the Baja British Columbia hypothesis. J. Geophys. Res. 109. http://dx.doi.org/10.1029/2003JB002696.

King, R.F., 1955. The remanent magnetism of artificially deposited sediments. Geophys. J. Int. 7, 115-134.

Kirschvink, J.L., 1980. The least-square line and plane and the analysis of paleomagnetic data. Geophys. J. R. Astron. Soc. 62, 699–718.

Knipper, A.L., Khain, E.V., 1980. Structural position of ophiolites of the Caucasus. Ofioliti 2 (Special Issue), 297–314.

Knipper, A.L., Ricou, L.-E., Dercourt, J., 1986. Ophiolites as indicators of the geodynamic evolution of the Tethyan ocean. Tectonophysics 123, 213–240.

Kodama, K.P., 2012. Paleomagnetism of Sedimentary Rocks: Process and Interpretation. Wiley-Blackwell (157 pp.).

Krasa, D., Petersen, K., Petersen, N., 2007. Variable field translation balance. Encyclopedia of Earth Sciences Series. In: Gubbins, D., Herrero-Bervera, E. (Eds.), Encyclopedia of Geomagnetism and Paleomagnetism.

Labails, C., Olivet, J.L., Aslanian, D., Roest, W.R., 2010. An alternative early opening scenario for the Central Atlantic Ocean. Earth Planet. Sci. Lett. 297 (3–4), 355–368. http://dx.doi.org/10.1016/j.epsl.2010.06.024.

Lefebvre, C.J.C., 2011. The tectonics of the Central Anatolian crystalline complex: a structural, metamorphic and paleomagnetic study. (PhD thesis). Utrecht University 978-90-6266-283-8.

Lefebvre, C., Meijers, M.J.M., Kaymakci, N., Peynircioglu, A., Langereis, C.G., van Hinsbergen, D.J.J., 2013. Reconstructing the geometry of central Anatolia during the late Cretaceous: large-scale Cenozoic rotations and deformation between the Pontides and Taurides. Earth Planet. Sci. Lett. 366, 83–98. http://dx.doi.org/10.1016/j.epsl.2013.01.003.

Liu, Q., Yu, Y., Torrent, J., Roberts, A.P., Pan, Y., Zhu, R., 2006. Characteristic low-temperature magnetic properties of aluminous goethite [α-(Fe, Al)OOH] explained. J. Geophys. Res. 111, B12S34. http://dx.doi.org/10.1029/2006JB004560.

Luterbacher, H.P., Ali, J.R., Brinkhuis, H., Gradstein, F.M., Hooker, J.J., Monechi, S., Ogg, J.G., Powell, J., Röhl, U., Sanfilippo, A., Schmitz, B., 2004. The Paleogene period. In: Gradstein, F.M., Ogg, J.G., Smith, A.G. (Eds.), A Geologic Time Scale 2004. Cambridge University Press, Cambridge, pp. 384–408.

Mandalyan, R., 1990. The Late Jurassic and Neocomian sedimentology and lithogenesis in Armenia. Publishing House of the AS of the Armenian SSR, Yerevan (173 pp., (in Russian)).

McFadden, P.L., McElhinny, L.W., 1988. The combined analysis of remagnetization circles and direct observations in palaeomagnetism. Earth Planet. Sci. Lett. 87, 161–172.

McFadden, P.L., McElhinny, M.W., 1990. Classification of the reversal test in palaeomagnetism. Geophys. J. Int. 103, 725–729.

Meijers, M.J.M., Hamers, M.F., Van Hinsbergen, D.J.J., Van der Meer, D.G., Kitchka, A., Langereis, C.G., Stephenson, R.A., 2010a. New late Paleozoic paleopoles from the Donbas Foldbelt (Ukraine): implications for the Pangea A vs. B controversy. Earth Planet. Sci. Lett. 297, 18–33.

Meijers, M.J.M., Langereis, C.G., Van Hinsbergen, D.J.J., Kaymakci, N., Stephenson, R.A., Altiner, D., 2010b. Jurassic–Cretaceous low paleolatitudes from the circum-Black Sea region (Crimea and Pontides) due to True Polar Wander. Earth Planet. Sci. Lett. 296, 210–226.

Meijers, M.J.M., Kaymakci, N., Van Hinsbergen, D.J.J., Langereis, C.G., Stephenson, R.A., Hippolyte, J.-C., 2010c. Late Cretaceous to Paleocene oroclinal bending in the Central Pontides (Turkey). Tectonics 29, TC4016. http://dx.doi.org/10.1029/2009TC002620.

Meijers, M.J.M., Van Hinsbergen, D.J.J., Dekkers, M.J., Altiner, D., Kaymakci, N., Langereis, C.G., 2011. Pervasive Palaeogene remagnetization of the central Taurides fold-and-thrust belt (southern Turkey) and implications for rotations in the Isparta Angle. Geophys. J. Int. 184, 1090–1112. http://dx.doi.org/10.1111/j.1365-246X.2010.04919.x.

Menning, M., Alekseev, A.S., Chuvashov, B.I., Davydov, V.I., Devuyst, F.-X., Forke, H.C., Grunt, A., Hance, L., Heckel, P.H., Izokh, N.G., Jin, Y.-G., Jones, P.J., Kotlyar, G.V., Kozur, H.W., Nemyrovska, T.I., Schneider, J.W., Wang, X.-D., Weddige, K., Weyer, D., Work, D.M., 2006. Global time scale and regional stratigraphic reference scales of Central and West Europe, East Europe, Tethys, South China, and North America as used in the Devonian–Carboniferous–Permian Correlation Chart 2003 (DCP 2003). Palaeogeogr. Palaeoclimatol. Palaeoecol. 240, 318–372. http://dx.doi.org/10.1016/j.palaeo.2006.03.058.

Merrill, R.T., McFadden, P.L., 2003. The geomagnetic axial dipole field assumption. Phys. Earth Planet. Inter. 139, 171–185.

Moix, P., Beccaletto, L., Kozur, H.W., Hochard, C., Rosselet, F., Stampfli, G.M., 2008. A new classification of the Turkish terranes and sutures and its implications for the paleotectonic history of the region. Tectonophysics 451, 7–39.

Monin, A.S., Zonenshain, L.P. (Eds.), 1987. History of the Ocean Tethys. Moscow Institute of Oceanology (in Russian).

Moskowitz, B.M., Frankel, R.B., Bazylinski, D.A., Jannasch, H.W., Lovley, D.R., 1989. A comparison of magnetite particles produced anaerobically by magnetotactic and dissimilatory iron-reducing bacteria. Geophys. Res. Lett. 16, 665–668. http://dx.doi.org/10.1029/GL016i007p00665.

Müller, R.D., Royer, J.-Y., Lawver, L.A., 1993. Revised plate motions relative to the hotspots from combined Atlantic and Indian Ocean hotspot tracks. Geology 21 (3), 275–278.

Nalivkin, P.V. (Ed.) 1976. Geological Map of Caucasus at 1/500 000 scale. Ministry of geology, USSR, Cief. Norton, I.O., 2000. Global hotspot reference frames in plate motion. In: Richards, M.A., Gordon, R.G., van der Hilst, R.D. (Eds.), The History and Dynamics of Global Plate Motion, 339–357.

Norton, I.O., 2000. Global hotspot reference frames and plate motion. In: Richards, M.A., Gordon, R.G, der Hilst, Van (Eds.), The history and dynamics of global plate motions 121. AGU Geophysical Monograph, Washington, pp. 339–357.

Ogg, J.G., Ogg, G., Gradstein, F.M., 2008. The Concise Geologic Time scale. Cambridge University Press 150 pp.

Ogg, J.G., Agterberg, F.P., Gradstein, F.M., 2004. The Cretaceous period. In: Gradstein, F.M., Ogg, J.G., Smith, A.G. (Eds.), A Geologic Time Scale 2004. Cambridge University Press, Cambridge, pp. 344–383.

Okay, A.I., Şahintürk, Ö., 1997. Geology of the Eastern Pontides. In: Robinson, A.G. (Ed.), Regional and Petroleum Geology of the Black Sea and Surrounding Region. AAPG Memoir, pp. 291–311.

Okay, A.I., Tüysüz, O., 1999. Tethyan sutures of northern Turkey. In: Durand, B., Jolivet, L., Horváth, F., Séranne, M. (Eds.), The Mediterranean Basins: Tertiary Extension Within the Alpine Orogen. Geological Society of London, Special Publications 156, pp. 475–515.

Paffenholtz, K.N., 1959. Geological History of the Caucasus. Izdatelstvo NAS Armenia SSR ((in Russian), 506 pp.).

Richards, M.A., Duncan, R.A., Courtillot, V.E., 1989. Flood basalts and hotspot tracks: plume heads and tails. Science 246, 103–107.

Robertson, A.H.F., Ustaomer, T., Pickett, E.A., Collins, A.S., Andrew, T., Dixon, J.E., 2004. Testing models of Late Palaeozoic–Early Mesozoic orogeny in Western Turkey: support for an evolving open-Tethys model. J. Geol. Soc. Lond. 161, 501–511.

Robertson, A.H.F., Parlak, O., Ustaomer, T., Taslıd, K., İnand, N., Dumitricae, P., Karaoğlan, F., 2014. Subduction, ophiolite genesis and collision history of Tethys adjacent to the Eurasian continental margin: new evidence from the Eastern Pontides, Turkey. Geodin. Acta http://dx.doi.org/10.1080/09853111.2013.877240.

Robinson, A.G., Banks, C.J., Rutherford, M.M., Hirst, J.P.P., 1995. Stratigraphic and structural development of the Eastern Pontides, Turkey. J. Geol. Soc. Lond. 152, 861–872. http://dx.doi.org/10.1144/gsjgs.152.5.0861.

Rolland, Y., Billo, S., Corsini, M., Sosson, M., Galoyan, G., 2009a. Blueschists of the Amassia–Stepanavan Suture Zone (Armenia): linking Tethys subduction history from E-Turkey to W-Iran. Int. J. Earth Sci. 98 (3), 533–550. http://dx.doi.org/10.1007/s00531-007-0286-8.

Rolland, Y., Galoyan, Gh., Bosch, D., Sosson, M., Corsini, M., Fornari, M., Vérati, C., 2009b. Jurassic Back-arc and hot-spot series in the Armenian ophiolites — implications for the obduction process. Lithos 112, 163–187.

Rolland, Y., Galoyan, G., Sosson, M., Melkonian, R., Avagyan, A., 2010. The Armenian ophiolites: insights for Jurassic Back-arc formation, Lower Cretaceous hot-spot magmatism, and Upper Cretaceous obduction over the South Armenian Block. In: Sosson, M., Kaymakci, N., Stephenson, R., Bergerat, F., Storatchenoko, V. (Eds.), Sedimentary Basin Tectonics from the Black Sea and Caucasus to the Arabian Platform. Geological Society of London, Special Publication 340, pp. 353–382.

Rolland, Y., Sosson, M., Adamia, Sh., Sadradze, N., 2011. Prolonged Variscan to Alpine history of an active Eurasian margin (Georgia, Armenia) revealed by $^{40}Ar/^{39}Ar$ dating. Gondwana Res. 20, 798–815.

Rolland, Y., Perincek, D., Kaymakci, N., Sosson, M., Barrier, E., Avagyan, A., 2012. Evidence for ~80–75 Ma subduction jump during Anatolide–Tauride–Armenian block accretion and ~48 Ma Arabia–Eurasia collision in Lesser Caucasus–East Anatolia. J. Geodyn. 56–57, 76–85.

Sahabi, M., Aslanian, D., Olivet, J.-L., 2004. A new starting point for the history of the central Atlantic. Compt. Rendus Geosci. 336 (12), 1041–1052.

Şengör, A.M.C., Yilmaz, Y., 1981. Tethyan evolution of Turkey: a plate tectonic approach. Tectonophysics 75 (3–4), 181–241.

Sokolov, S.D., 1977. The Olistostromes and Ophiolitic Nappes of the Lesser Caucasus. Izdatelstvo 'Nauka', Moscow (in Russian).

Sosson, M., Rolland, Y., Muller, C., Danelian, T., Melkonyan, R., Kekelia, M., Adamia, S.A., Babazadeh, V., Kangarli, T., Avagyan, A., Galoyan, G., Mosar, J., 2010. Subduction, obduction and collision in the Lesser Caucasus (Armenia, Azerbaijan, Georgia), new insights. In: Sosson, M., Kaymakci, N., Stephenson, R.A., Bergerat, F., Starostenko, V. (Eds.), Sedimentary Basin Tectonics from the Black Sea and Caucasus to the Arabian Platform. Geological Society of London, Special Publications, London 340, pp. 329–352. http://dx.doi.org/10.1144/SP340.14 0305-8719/10.

Stampfli, G.M., Borel, G.D., 2002. A plate tectonic model for the Paleozoic and Mesozoic constrained by dynamic plate boundaries and restored synthetic oceanic isochrons. Earth Planet. Sci. Lett. 196 (1–2), 17–33.

Sun, W.W., Kodama, K.P., 1992. Magnetic anistropy, scanning electron microscopy, and X-ray pole figure goniometry study of inclination shallowing in a compacting clay-rich sediment. J. Geophys. Res. 97, 19599–19615.

Tan, X., Kodama, K.P., 2003. An analytical solution for correcting paleomagnetic inclination error. Geophys. J. Int. 152, 228–236.

Tan, X., Kodama, K.P., Fang, D., 2002. Laboratory depositional and compaction-caused inclination errors carried by haematite and their implications in identifying inclination error of natural remanence in red beds. Geophys. J. Int. 151, 475–486.

Tauxe, L., Kent, D.V., 1984. Properties of a detrital remanence carried by hematite from study of modern river deposits and laboratory redeposition experiments. Geophys. J. R. Astron. Soc. 76, 543–561.

Tauxe, L., Kent, D.V., 2004. A simplified statistical model for the geomagnetic field and the detection of shallow bias in paleomagnetic inclinations: was the ancient magnetic field dipolar? In: Channell, J.E.T., Kent, D.V., Lowrie, W., Meert, J.G. (Eds.), Timescales of the Paleomagnetic Field 145. AGU Geophysical Monograph, Washington, pp. 101–115

Tauxe, L., Watson, G.S., 1994. The foldtest: an eigen analysis approach. Earth Planet. Sci. Lett. 122, 331–341.

Tauxe, L., Kodama, K.P., Kent, D.V., 2008. Testing corrections for paleomagnetic inclination error in sedimentary rocks: a comparative approach. Phys. Earth Planet. Inter. 169, 152–165.

Topuz, G., Altherr, R., Siebel, W., Schwarz, W.H., Zack, T., Hasözbek, A., Barth, M., Satır, M., Şen, C., 2010. Carboniferous high-potassium I-type granitoid magmatism in the Eastern Pontides: the Gümüşhane pluton (NE Turkey). Lithos 116, 92–110. http://dx.doi.org/10.1016/j.lithos.2010.01.003.

Torsvik, T.H., et al., 2012. Phanerozoic polar wander, palaeogeography and dynamics. Earth Sci. Rev. 114, 325–368.

Van der Voo, R., 1968. Jurassic Cretaceous and Eocene pole positions from northeastern Turkey. Tectonophysics 6, 251–269. http://dx.doi.org/10.1016/0040-1951(68)90053-X.

Van Hoof, A.A.M., Langereis, C.G., 1991. Reversal records in marine marls and delayed acquisition of remanent magnetization. Nature 351, 223–224.

Van Velzen, A.J., Zijderveld, J.D.A., 1995. Effects of weathering on single domain magnetite in early Pliocene marls. Geophys. J. Int. 121, 267–278.

Watson, G., 1983. Large sample theory of the Langevin distributions. Journal of Statistical Planning and Inference. 8, 245–256.

Zakariadze, G.S., Karpenko, S.F., Bazylev, B.A., Adamia, S.A., Oberhaensli, R.E., 1998. Petrology, geochemistry, and Sm–Nd age of the pre-late Variscan paleooceanic complex of the Dzirula salient, Transcaucasian massif. Petrology 6, 388–408 (translated from Petrologiya, 6, 422-444).

Zijderveld, J.D.A., 1967. A. C. demagnetization of rocks: analysis of results. In: Collinson, D.W., Creer, K.M., Runcorn, S.K. (Eds.), Methods in Palaeomagnetism. Elsevier, Amsterdam, New York, pp. 254–286.